Universität Hamburg
DER FORSCHUNG | DER LEHRE | DER BILDUNG

Department of Earth Sciences
University of Hamburg
Summer semester 2016

Bachelor Thesis

Local Structure and Dynamics of the Ferroelectric $(1-x)PbTiO_3-xBiMg_{0.5}Ti_{0.5}O_3$ with $x=0.20$ studied by Raman Spectroscopy

Irina Margaritescu
September 24, 2016

Supervised by
PD. Dr. Boriana Mihaylova
Dr. Kaustuv Datta

Local structure and dynamics of the ferroelectric $(1-x)PbTiO_3 - xBiMg_{0.5}Ti_{0.5}O_3$ with $x = 0.20$ studied by Raman spectroscopy

Abstract

Piezoelectric ceramics play an important role in the development of new electronic devices, with lead zirconate titanate being currently one of the most used piezoelectric ceramic materials. However, numerous studies over the last decades have classified lead as damaging for the human health and the environment. For that reason, lead-free and lead-poor ferroelectrics have been gaining increasing attention in the last few years, but despite extensive research no compound with similar properties to PZT has been found yet. The solid solution (1-x)$PbTiO_3$-x$BiMeO_3$ with Me=$Mg_{0.5}Ti_{0.5}$, $Ni_{0.5}Ti_{0.5}$, $Co_{0.5}Ti_{0.5}$ etc. exhibits promising piezoelectric properties at the morphotropic phase boundary, where a composition-driven phase transition occurs and could offer a lead-poor alternative to PZT, but is has been insufficiently studied until now.

In this thesis the local structure and atomic dynamics of the solid solution (1-x)$PbTiO_3$-x$BiMg_{0.5}Ti_{0.5}O_3$ with x=0.20 and $PbTiO_3$ are analyzed by Raman spectroscopy on cooling from 870K to 100K and 130K, respectively. The temperature-induced transformations in 0.8$PbTiO_3$-0.2$BiMg_{0.5}Ti_{0.5}O_3$ and $PbTiO_3$ are compared and discussed. The results show that by adding $BiMg_{0.5}Ti_{0.5}O_3$ to pure $PbTiO_3$ local distortions in the lattice appear. The ferroelectric phase transition is driven by the softening of the phonon modes around 88 cm^{-1}, 125cm^{-1}, 153cm^{-1} and 290cm^{-1}; atomic displacements of the A-site and B-site cations can also be observed above the transition temperature, which indicates the presence of both displacive and order/disorder phenomena.

Table of contents

List of Figures

1 Introduction

A material is said to be ferroelectric if it exhibits spontaneous polarisation in the absence of an external electric field and has the ability to flip between different states of electric polarisation by the application of an electric field. Ferroelectricity was discovered at the beginning of the 1920s in sodium potassium tartrate tetrahydrate ($KNaC_4H_4O_6 \cdot 4H_2O$), also known as Rochelle salt, by the American physicist Joseph Valasek.[5] The name was chosen by analogy with ferromagnetism, because of the similar properties of ferromagnetic and ferroelectric materials. They both exhibit a spontaneous magnetic/dipole moment in the ferroic state and have a hysteresis loop. However, ferroelectrics have a different fundamental mechanism than ferromagnetics and are used for different applications.[16]

An important step in the research was made in the 1940s with the discovery of ferroelectricity in the polycrystalline ceramic barium titanate ($BaTiO_3$) from the perovskite family, which became one of the most used ferroelectric materials.[31] Researchers became interested in other compounds with the perovskite structure type, in which the ferroelectric mechanism was easier to understand than in the previously known hydrogen-bonded ferroelectrics.[5]

Nowadays ferroelectrics have a great variety of applications in the electronic industry, for example as capacitors, memories or high-energy pulse generators,[16] in medical devices, such as insulin pumps and ultrasonic cataract-removal devices, or in the automotive industry, as airbag sensors and seat belt buzzers.[24]

One of the most used piezoelectric ceramic worldwide is the solid solution lead zirconate titanate (PZT). However, several studies over the last decades have classified lead as damaging for the human health and the environment and new regulations in the EU are trying to restrict the use of lead. For that reason, lead-free and lead-poor ferroelectrics have been gaining increasing attention in the last few years, but despite extensive research no compound with similar piezoelectric properties to PZT has been found yet.[33]

This calls for further fundamental studies of the structure and lattice dynamics of various ferroelectric solid solutions in order to clarify the relation chemistry-structure-properties. The aim of this thesis is to apply Raman spectroscopy in order to analyze the temperature-induced structural transformations and coupling processes in a novel solid solution with a reduced amount of lead. This solid solution is (1-x)$PbTiO_3$-x$BiMg_{0.5}Ti_{0.5}O_3$ with x=0.20. Its atomic dynamics in the paraelectric and ferroelectric phase and at a phase transition will be compared to the one of pure $PbTiO_3$, a well known ferroelectric material.

This thesis is structured in six chapters. Chapter 2 gives an introduction to the fundamentals of ferroelectricity. Chapter 3 makes a brief description of industrial relevant piezoelectric ceramics and the morphotropic phase boundary. Chapter 4 offers an overview of the experimental techniques used to analyze the samples and the methods used for data evaluation. In Chapter 5 the results are presented and discussed. Chapter 6 presents the conclusions of this thesis.

2 Theoretical concepts of ferroelectricity

This chapter will introduce different concepts of ferroelectricity. A short description of ferroelectric materials will be given in Chapter 2.1. This thesis focuses on one certain type of ferroelectric structure, the perovskite structure, which will be discussed in Chapter 2.2. Further, the behaviour of the polarisation with respect to the electric field will be described in Chapter 2.3. Theoretical principles of lattice dynamics will be discussed in Chapter 2.4, followed by a classification of ferroelectrics based on the behaviour of the order parameter at a phase transition (Chapter 2.5) and on the changes in the symmetry that take place at the Curie temperature (Chapter 2.6).

2.1 Definition of ferroelectricity

Crystals are classified into 32 crystallographic point groups, or crystal classes, based on their symmetry with respect to a point. 21 of this crystal classes do not have a center of symmetry and they are, with one exception, piezoelectric, which means that an applied mechanical stress will cause a change in the polarisation. 10 classes of these piezolectric crystals are polar classes; they possess a unique axis of symmetry with no mirror plane perpendicular to it (polar axis). Hence the primitive unit cell of such crystals exhibits a spontaneous polarisation which can be influenced by variations in temperature. These are called pyroelectric crystals. If the direction of the spontaneous polarization can be changed by an applied electric field, then the crystals are also ferroelectric (Figure 1). More precisely, a ferroelectric material is defined by the presence of two or more stable states of different electric polarisation in absence of an external electric field and the ability to switch between the states under the application of an electric field.[5]

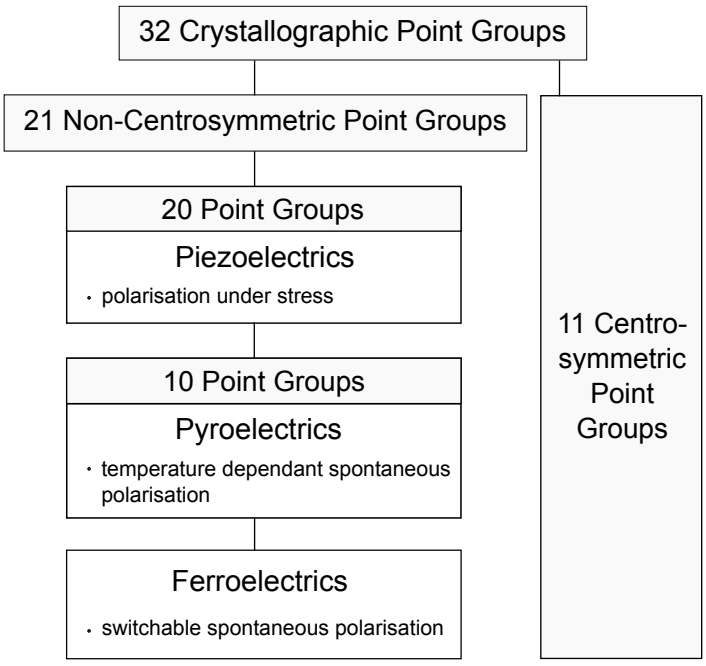

Figure 1: The 32 Crystallographic Point Groups. Ferroelectric materials are also piezoelectric and pyroelectric.

Ferroelectric materials can be classified by their structure:

a. Inorganic oxides containing corner-sharing BO_6 octahedra, with B-site cation being a d^0 element (commonly Ti, Ta or Nb) - for example the perovskite oxide compounds, which will be discussed in Chapter 2.2,

b. Hydrogen bounded compounds and

c. Ferroelectric polymers,[6]

or by their behaviour during a phase transition (Chapter 2.5).

2.2 The perovskite structure

The perovskite family has been named after the mineral perovskite ($CaTiO_3$) and is a group of compounds that share the same general stoichiometry: ABX_3. Perovskites have the ability to accommodate a great variety of chemical elements and undergo multiple structural transformations. The simplicity of their structure allowed for a deeper understanding of ferroelectricity and the interesting physical and chemical characteristics they exhibit brought them to the focus of researchers since the middle of the 20th century.[22]

2.2.1 The idealised structure

The perovskite structure has the general formula ABX_3, where A and B are two cations with different ionic radii size and X is an anion. This thesis is focusing on the perovskite oxide compounds, where the anion site is occupied by oxygen, therefore only the case of ABO_3 compounds will be discussed. In the ideal perovskite lattice the larger A-site cation is placed at the center of the cubic unit cell and it is 12-fold coordinated by oxygen. The smaller B-site atoms occupy the cube corners and are 6-fold octahedrally coordinated by oxygen. (Figure 2a)

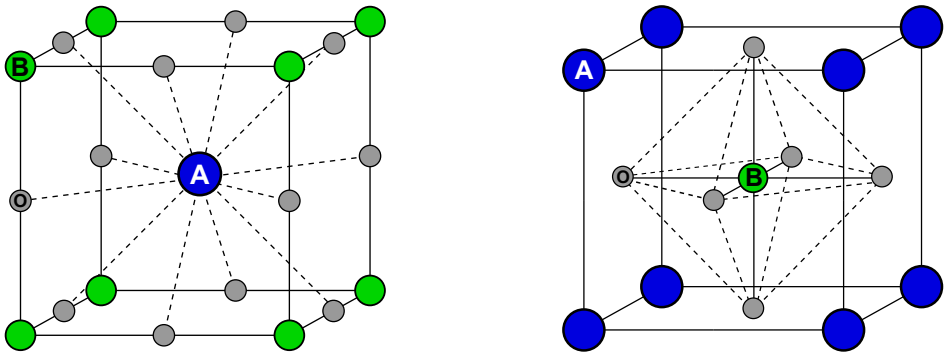

(a) (b)

Figure 2: Two different representations of the unit cell of the ideal cubic perovskite structure (space group $Pm\bar{3}m$). The position of the atoms in the unit cell is given in fractional coordinates: (a) A$(\frac{1}{2},\frac{1}{2},\frac{1}{2})$, B$(0,0,0)$ and the three oxygen atoms: $(\frac{1}{2},0,0)$, $(0,\frac{1}{2},0)$, $(0,0,\frac{1}{2})$. (b) A$(0,0,0)$, B$(\frac{1}{2},\frac{1}{2},\frac{1}{2})$ and O: $(\frac{1}{2},\frac{1}{2},0)$, $(0,\frac{1}{2},\frac{1}{2})$, $(\frac{1}{2},0,\frac{1}{2})$.

2.2.2 Phase transitions in perovskites

The idealised version of the perovskite lattice is typical of the high-temperature, paraelectric phase. At room temperature most of the ABO_3 compounds are distorted from the ideal cubic structure (spacegroup $Pm\bar{3}m$) to a lower symmetry. This distortion is also the origin of spontaneous polarisation, which is generated by the displacement of positive and negative charge centers.[22] During a phase transition the point group usually changes from $m\bar{3}m$ to $4mm$ and the 3−fold axes and the center of symmetry disappear.[14] However, the ferroelectric state in perovskite-type materials can also have rhombohedral, orthorhombic or even monoclinic symmetry.

Trying to understand the nature of the multiple structural transformations in perovskites, the Swiss mineralogist Victor Goldschmidt analyzed the behaviour of the lattice with regard to the ionic radii and discovered that in an idealised cubic structure the atoms obey the following rules:

a. a central cation is surrounded and touched by as many anions as possible,

b. all the anions must touch the cations and

c. the anion-cation distance is equal the sum of their ionic radii.

Based on these criteria, he described the relation between atoms in an idealised cubic structure with the help of the following formula:

$$r_A + r_O = \sqrt{2}(r_B + r_O) \tag{2.1}$$

where r_A is the ionic radius of A, r_B is the ionic radius of B and r_O is the ionic radius of oxygen.[22]

Because in nature it is unlikely to find a perfect size-matching pair of A and B cations, usually there will be a small mismatch, which leads to a structural distortion.[14] In order to measure the degree of the deviation from the ideal unit cell, Goldschmidt introduced the tolerance factor:

$$t = \frac{r_A + r_O}{\sqrt{2}(r_B + r_O)} \tag{2.2}$$

If $t = 1$, the compound will have the ideal cubic structure. If $t > 1$, the B cation is too small for its site and can move from the center of the oxygen cage, which leads to a small polar distortion (Figure 3a). This materials are called B-site driven and usually have a rhombohedral structure.[19,22] A tolerance factor slightly under 1 indicates that the A atom is smaller than the ideal value and doesn't touch all 12 surrounding oxygen atoms. As a consequence the BO_6 ochtahedra will tilt and rotate in order to fill the space (Figure 3b). Since in this case the inversion symmetry is preserved, the so called A-site driven materials are generally not ferroelectric. An exception are compounds with Pb^{2+} as A cation.[19]

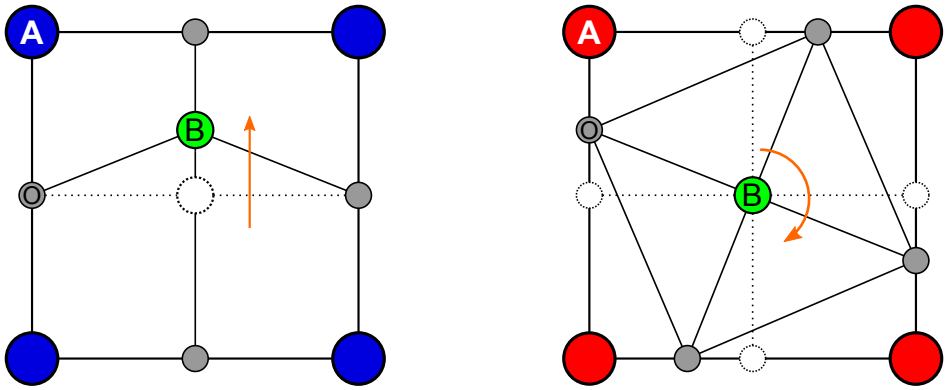

(a) (b)

Figure 3: A- and B-site driven lowering of the symmetry. (a) B-site driven ferroic polar structural distortion . The B-cation moves in one of the six possible directions. (b) A-site driven ferroic non-polar structural distortion. Rotation of the BO_6 octahedra.

2.3 Domains and hysteresis loop

In a ferroelectric material the polarisation is not uniform throughout the entire bulk of the specimen. Small regions containing a large amount of dipoles with the same orientation spontaneously form during a phase transition. This regions are called ferroelectric domains and the boundaries between them are called domain walls. In order to minimize the total energy of the crystal, different domains are oriented in such a way that their polarisation will compensate for each other and the net polarisation of the crystal may be zero or close to zero.[16] It should be emphasized that domains are not polycrystalline grains. If not poled, a single crystal is composed of domains whose orientation follow the symmetry allowed crystallographic directions, e.g. for a tetragonal phase these are all cubic $\langle 100 \rangle$. Polycrystalline grains are randomly oriented, and a single grain can in turn be composed of several domains.

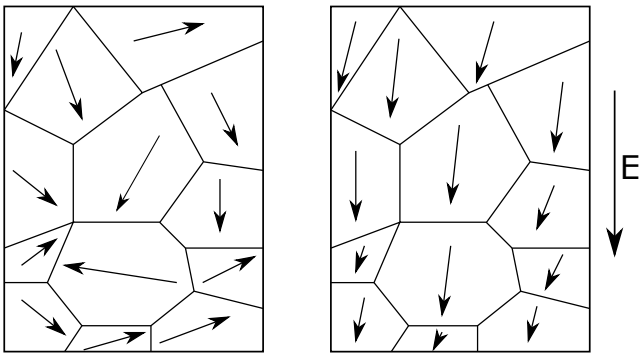

Figure 4: A sketch of domains in a ferroelectric material before (left) and after (right) the application of an electric field

When an external electric field is applied, the domains will start to change their orientation in one direction (Figure 4). By reversing the external field, the direction of the domains changes too, but with a small lag after the change in the external electric field.[1] This lag of the electric polarization is called ferroelectric hysteresis.

The hysteresis appears in certain temperature regions, delimited by the Curie temperature.[16] When an external electric field is applied, the domains are starting to orient in the

direction of the field (path AB) (Figure 5). Between B and C the polarisation has reached a state of saturation, and almost all domains are aligned towards the direction of the field. The polarisation is then decreasing with the electric field following the path CBD. OE represents the spontaneous polarisation and OD the remanent polarisation at E=0. The remanent polarisation is smaller than the spontaneous polarisation because some of the domains are returning to their original orientations in the absence of an external field.[16]

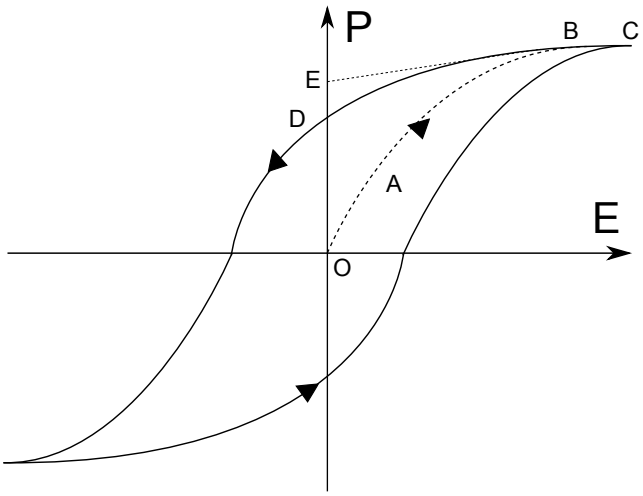

Figure 5: Polarisation as a function of electric field. Plot of a hysteresis loop.

2.4 Lattice dynamics and the soft mode theory

A crystal lattice is a periodic array of atoms. When the equilibrium of the system is disturbed, small displacements of the atoms take place, causing vibrations of the lattice. The quanta of this lattice vibrations are called phonons. Phonons can be treated as harmonic oscillators and have the energy $E = \hbar\omega$, where $\hbar$ is the Planck constant divided by 2π and ω is the angular frequency of the vibration.[14]
In a crystal with more than two different atoms there are two types of phonons: acoustic and optical. In the acoustic branch, adjacent different atoms vibrate in the same direction with a periodically varying amplitude. In the optical branch, different adjacent atoms vibrate in opposite directions with amplitudes inversely proportional to the atom masses. The frequency of the atomic vibrations depends on the wave vector k.[13]

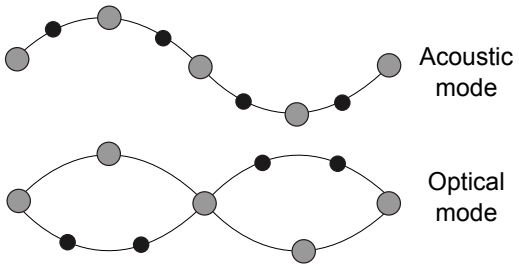

Figure 6: Acoustic and optical phonon modes.

The optical and acoustic branches are divided into longitudinal and transverse modes. Longitudinal waves are created by atoms that are displaced along the direction of propagation

of the wave. Transverse waves are created by atoms that are displaced normal to the wave propagation direction.[13] Figure 6 displaces transverse acoustic and optical modes. In a crystal with n different atoms in the primitive unit cell, there are $3n$ phonon branches. Three branches are acoustic phonons: one longitudinal (LA) and two transverse (TA). The other $3n - 3$ branches are optical phonons, which are also divided in longitudinal and transverse modes (LO and TO).

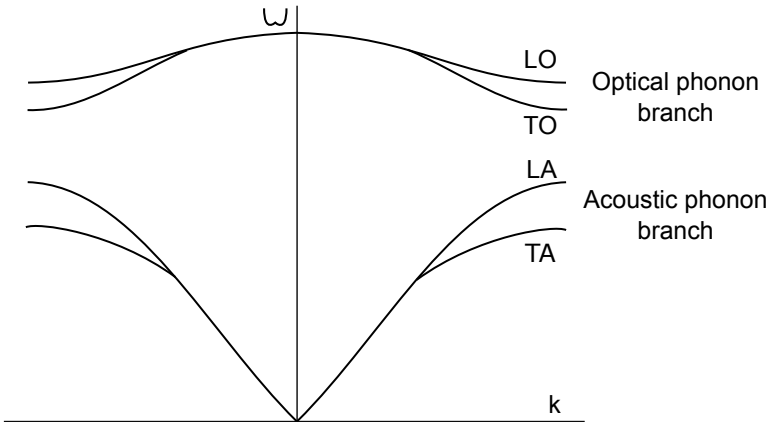

Figure 7: Dispersion curves for a crystal with two different atoms. Acoustic phonons have a lower energy than optical phonons.[13]

2.4.1 The soft mode

When a crystal undergoes a transition from a higher to a lower symmetry phase, there can be a particular phonon, whose characteristic frequency ω decreases to zero as the transition is approached. This particular mode of the crystal lattice is called the soft mode and its frequency is said to soften.[4] This softening occurs because anharmonic interactions in the crystal cause a temperature renormalization of the phonon frequencies. The atomic motions associated with the soft mode correspond to the way the structure distorts through a phase transition.[14] The structure of the new phase is determined by the structure of the parent (paraelectric) phase and the eigenvector of the soft mode, which is the array of atomic displacements relative to the lattice sites.[4]

In the ferroelectric perovskites the soft mode involves the cations moving in opposite directions to the anions.[14]

2.5 Landau theory of phase transitions

Apart from their structure, ferroelectrics can also be classified based on their behaviour at the phase transition. The Russian physicist Lev Landau distinguishes a first-order phase transition, which is abrupt and is followed by a temperature hysteresis and a second-order phase transition, which is continuous and is followed by a polarisation hysteresis.[6]
A ferroelectric phase transition can be described at a macroscopic level using the Landau model. Based on the theory that the thermodynamic equilibrium of a system can be described using different variables such as temperature, polarisation, strain and electric field, Landau expressed the free energy of a crystal as a power series in the order parameter.[5] In ferroelectrics the macroscopic order parameter is the polarisation and its behaviour determines

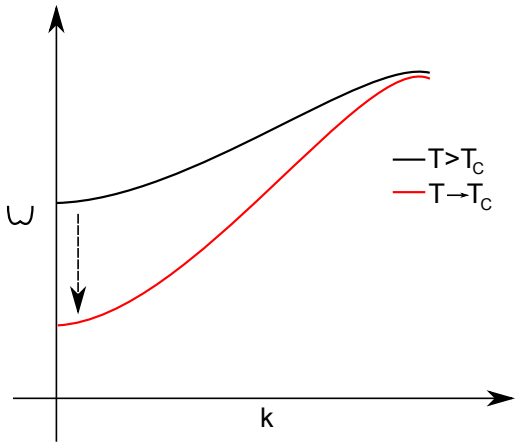

Figure 8: Behaviour of the ferroelectric soft mode.[14]

the type of the phase transition.

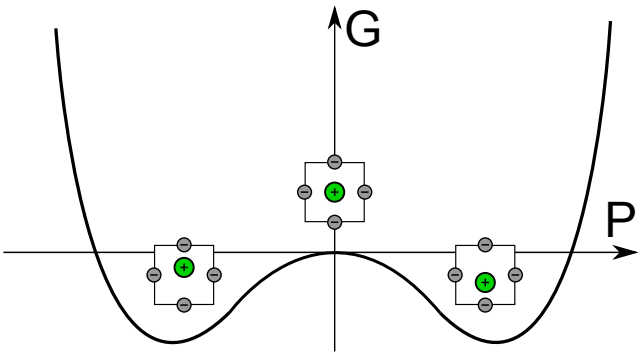

Figure 9: The free energy as a function of polarisation. The double potential well in a ferroelectric with two stable polarization states.

The power series can be written in form of the following simplified polynomial expression:

$$G = \frac{1}{2}\alpha P^2 + \frac{1}{4}\gamma P^4 + \frac{1}{6}\delta P^6, \tag{2.3}$$

where G is the free energy of the system, P is the polarisation, α is a temperature dependent coefficient, with $\alpha = \beta(T - T_C), \beta > 0$, and γ and δ are two temperature independent coefficients. T_C is the Curie temperature, where a material loses its ferroelectric properties and goes into the paraelectric state.

If a system can have several different states, it will choose the state with the lowest energy.[16] The minimum free energy of the system can be determined by differentiating Equation 2.3 with respect to P:

$$\frac{\partial G}{\partial P} = \alpha P + \gamma P^3 + \delta P^5 \tag{2.4}$$

and then solving Equation 2.4 under the condition that

$$\frac{\partial G}{\partial P} = 0. \tag{2.5}$$

The sign of γ determines the order of the phase transition.[5,21,34] This will be discussed in the following two Subchapters.

2.5.1 Second-order phase transition

If $\gamma > 0$, the system undergoes a second-order phase transition and the change in the spontaneous polarisation is continuous (Figure 10).

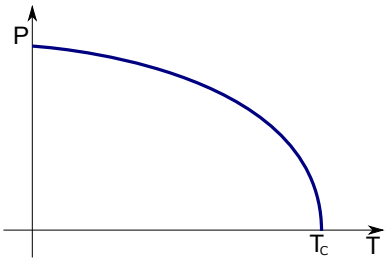

Figure 10: Polarisation as a function of temperature. On heating the order parameter decreases continuously to 0.

In case of a second-order transition, Equation 2.3 can be simplified[16] to:

$$G = \frac{1}{2}\alpha P^2 + \frac{1}{4}\gamma P^4, \tag{2.6}$$

and Equation 2.4, which was also adjusted, has the following solutions for temperatures below T_C: $P_1 = 0$, where the system has a local maximum and is therefore extremely unstable and $P_2 = -\sqrt{\frac{\alpha}{\gamma}}$ and $P_3 = \sqrt{\frac{\alpha}{\gamma}}$, for which the free energy curve G has two minima, which are the preferred stable states. When raising the temperature towards T_C, P_2 and P_3 will gradually near and become one minimum point at $P = 0$ for temperatures higher than T_C. Above T_C the unpolar state is more stable than the polar state (Figure 11).[14]

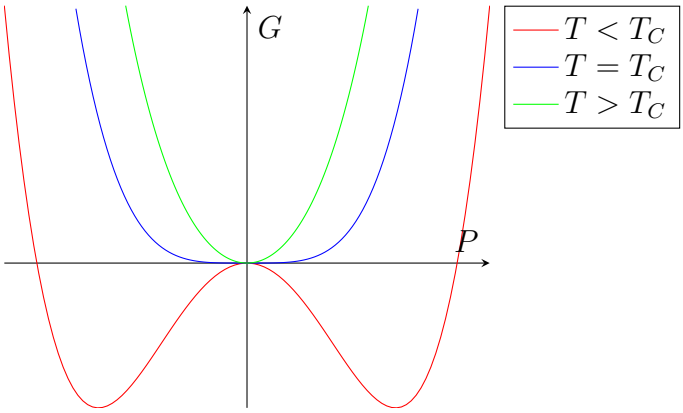

Figure 11: Free energy as a function of polarisation. The free energy of the system is stable above T_C and unstable under T_C.

2.5.2 First-order phase transition

For $\gamma < 0$, the system undergoes a first-order phase transition and there is a discontinuity in the order parameter (Figure 12), which drops to 0 from a finite value at the transition temperature.

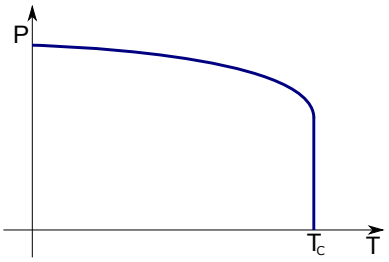

Figure 12: Polarisation as a function of temperature. On heating the order parameter changes abruptly to 0 at the transition temperature.

This type of transition is more complex than the previous one. In this case α is given by $\alpha = \beta(T - T_0)$, where T_0 is close, but not equal to the transition temperature T_C.[5] A first-order transition takes place when $G = 0$ and $\frac{\partial G}{\partial P} = 0$ and the transition temperature is

$$T_C = T_0 + \frac{3\gamma^2}{16\beta\delta}. \tag{2.7}$$

At $T = T_C$ Equation 2.4 has five solutions and the free energy curve G has three different minimum points. As the temperature is lowered below T_C, the ferroelectric state becomes more stable, but the paraelectric phase remains present until $T = T_0$, as a local minimum of G at $P = 0$.[21]
Experiments have shown that the actual transition occurs at a higher temperature if reached from a low temperature side. This is called thermal hysteresis.[5]

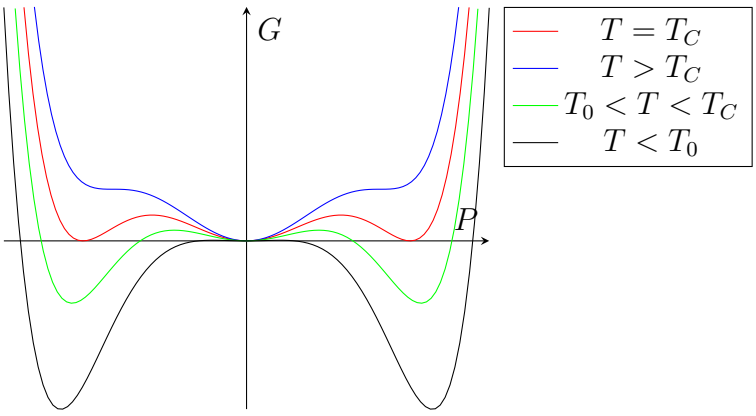

Figure 13: Free energy as a function of polarization in a first-order phase transition.

2.6 Displacive and order-disorder ferroelectrics

Another classification of ferroelectric materials is based on the changes in the symmetry that take place at the transition temperature:

a. a discrete symmetry group is broken at T_C: displacive and order-disorder ferroelectrics,

b. a continuous symmetry group is broken at T_C: ferroelectric liquid crystals and

c. no macroscopic symmetry is broken: relaxors.[20]

This thesis will only address the first case, in which a discrete symmetry group is broken. In a displacive phase transition the symmetry of the crystal is changed from a higher to lower phase by small atomic displacements. The atoms slightly change their position and dipole moments appear.[14] According to the Landau theory, in a displacive transition the order parameter disappears above the transition temperature, which means that the lattice displacements corresponding to the polarization are zero above T_C .[21] In the case of an order-disorder transition, the polarization has a non-zero finite value above T_C, but local symmetry-breaking distortions take place in every unit cell, with randomly changing direction at the transition temperature, so there is no net polarization.[21]

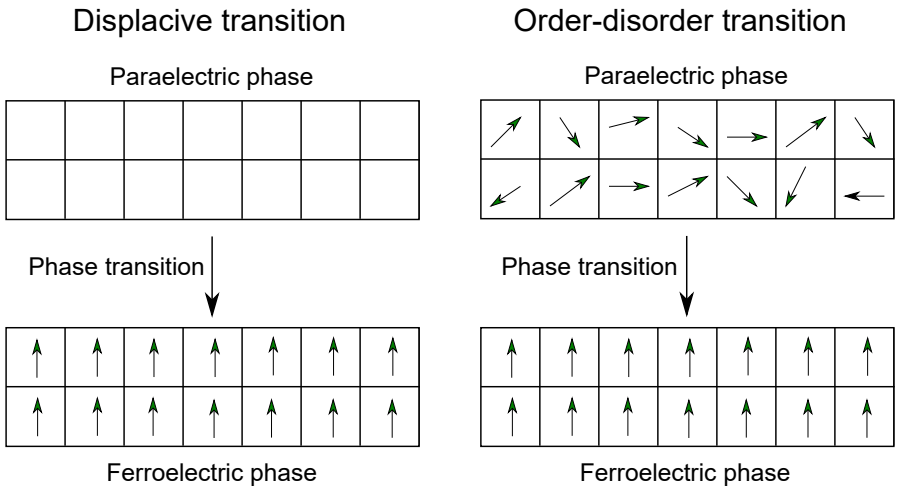

Figure 14: Displacive (left) and order-disorder (right) transition.

Initially, ferroelectrics have been considered as having either a displacive or an order-disorder transition, but recent studies have shown that most ferroelectric materials exhibit both displacive and order-disorder characteristics at a phase transition.[9]

3 Piezoelectric ceramics

Piezoelectric ceramics have been discovered in the 1950s[3] and have been playing an important role in the development of new electronic devices since then. Piezoelectric ceramic materials have a large field of applications including computers, medical sector and automobiles. Commonly used ceramics are barium titanate ($BaTiO_3$ - BT), lead titanate ($PbTiO_3$ - PT) and lead zirconate titanate ($Pb(Zr,Ti)O_3$ - PZT).[24]

Lead zirconate titanate is currently one of the most used piezoelectric ceramic materials. PZT is a solid solution between lead zirconate ($PbZrO_3$) and lead titanate. In a solid solution at least two types of atoms occupy the same crystallographic site. The initial crystal structure remains unchanged, without new structures being formed. The final product is influenced by different variables: atomic size factor, crystal structure, electronegativity and valences of the solute and solvent atoms.[24] These ceramics are used extensively for their excellent piezoelectric properties at the morphotropic phase boundary.[29]

However, new environmental regulations are recommending a reduced use of lead, and researchers have begun the search for lead-free piezoelectric materials. Bismuth titanate, bismuth sodium titanate and potassium niobate, together with their solid solutions, are some of the candidates for lead-free ceramics that have been actively studied in the last years. However, although they have a large piezoelectric constant which makes them suitable for actuators and high power applications, they also have disadvantages, such as a low Curie and depolarisation temperature and difficulties in poling treatments. Unfortunately, none of the previously studied lead-free materials has comparable piezoelectric properties to PZT.[33]

This thesis analyzes a new compound with reduced amount of lead, a solid solution of lead titanate and bismuth magnesium titanate: $(1\text{-}x)PbTiO_3\text{-}xBiMg_0.5Ti_0.5O_3$, with x=0.20. The obtaining process of this piezolectric ceramic will be discussed in Chapter 4. A detailed analysis of the Raman spectra will be made in Chapter 5.

3.1 The morphotropic phase boundary

All phase transitions described in Chapter 2 refer to transformation processes induced by variations in the temperature, but a change in the composition can also trigger a transition and induce changes in the structure of the crystal.

The transition between a tetragonal and a rhombohedral ferroelectric phase caused by a variation in the composition is described by the term “morphotropic phase boundary” (MPB) (Figure 15).[18,29]

Close to the MPB the structure of the crystal changes abruptly and the ferroelectric exhibits enhanced electromechanical properties.[28,29] Studies have shown that near the MPB the piezoelectric coefficients maximise due to:

a. “a peak in the spontaneous polarization, to which the intrinsic piezoelectric coefficient is proportional and

b. near degeneracy of the tetragonal and rhombohedral states, which allows for ease of reorientation of domains under applied fields and stresses, thereby maximising the extrinsic piezoelectric contributions”[18]

What makes the MPB attractive for researchers is the transition that can be achieved without the influence of other external variables like temperature or electric field.[28] Since

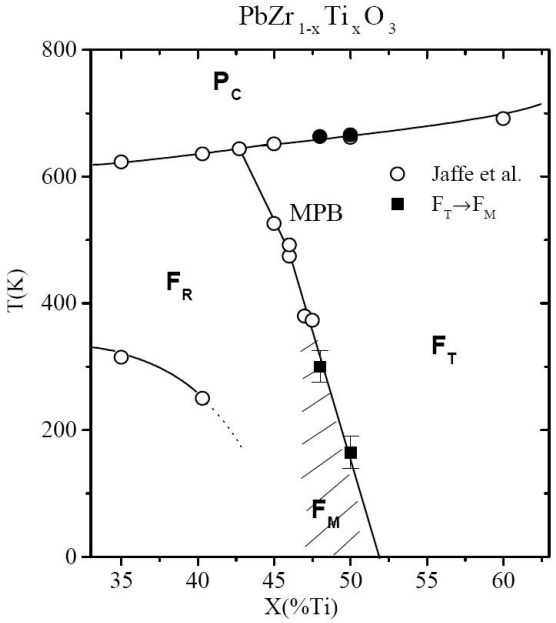

Figure 15: The phase diagram for lead zirconate titanate. The line dividing the rhombohedral (F_R) and tetragonal (F_T) phases is called the morphotropic phase boundary.[29]

the morphotropic phase boundary is considered the source of outstanding piezoelectric performance in ceramics, finding or tailoring materials with a similar phase boundary is one aspect current research is focusing on. Modern structural analysis revealed significant structural complexity near MBP. The composition-driven tetragonal-rhombohedral phase transition can be realized via an intermediate monoclinic/orthorhombic phase (polarization rotation model) or a coexistence of several phases. MPB can also occur between tetragonal and monoclinic phases.

3.2 $PbTiO_3$

Lead titanate belongs to the family of perovskite oxides and is a widely used material in the electronic industry, alone or as the end member in the solid solution PZT.[27]

The high-temperature paraelectric phase of $PbTiO_3$ has a cubic symmetry with a unit cell parameter $a = 3.9045$Å. In the ferroelectric tetragonal phase, the tetragonality is given by $\frac{c}{a} = 1.063$. The transition temperature is at 763K, where the crystal undergoes a first-order transition (Figure 16).[27]

Below the phase transition, the tetragonal structure is stabilised by the hybridization between the valence-electron states of Pb^{2+} cations and the O^{2-} anions, which leads to a large strain and induces the hybridization between the 3d electron states of Ti^{4+} cation and the 2p electron states of oxygen anions. This allows the Ti atoms to shift off the center of the oxygen cages, with both titanium atom and oxygen ochtahedron being displaced in the same direction with respect to the lead atom.[35] The phonon mode associated with the vibration of titanium cation in the center of the oxygen octahedra softens during the phase transition.[14]

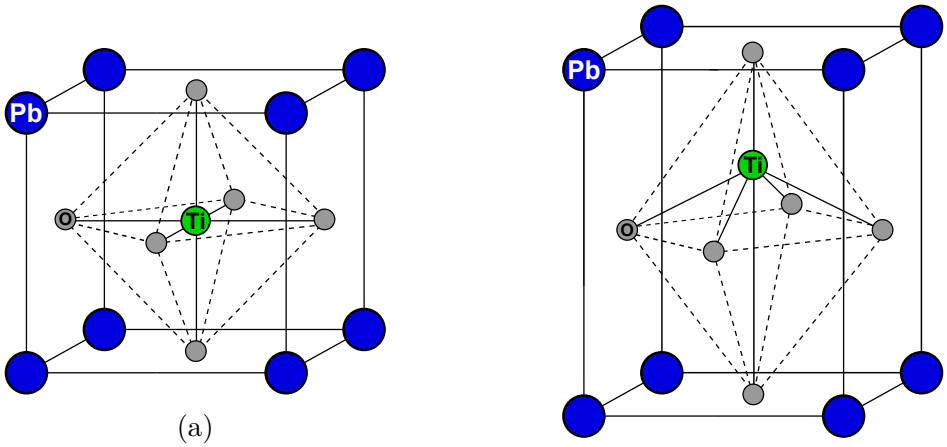

Figure 16: $PbTiO_3$ (a) in a paraelectric, cubic state and (b) in a ferroelectric, tetragonal state

Lead titanate has been considered for a long time to be a textbook example of a displacive transition,[5] but experiments made in the last years have shown that local distortions also exist above the transition temperature and there are evidences of an order-disorder behaviour in $PbTiO_3$.[9] A more detailed discussion on $PbTiO_3$ will take place in Chapter 5.

4 Methods

This chapter will give a short introduction to the theoretical principles of Raman spectroscopy followed by an the overview of the methods used for the sample preparation, data collection and data evaluation. At the end of this chapter we will use group-theory analysis in order to predict which vibrational modes in the paraelectric and ferroelectric phases of ABO_3-type compounds are Raman-active.

4.1 Raman spectroscopy

Vibrational spectroscopy is a widely used method in material science and can deliver a qualitative and quantitative structural information for different types of compounds with a broad range of physical states. The resulting spectra provide information about the structure and dynamics of the solid.[30] Two of the most used methods in the vibrational spectroscopy are infrared (IR) and Raman spectroscopy, which are complementary methods.

The vibrational energy levels in a molecule depend on the masses and arrangement of the atoms and the bonding between them. The combination of these characteristics is unique for a molecule, therefore measurements carried out by IR and Raman spectroscopy can provide a "fingerprint" for a molecule as well as of a solid.[30] The collectivized atomic vibrations in periodic solids, the phonons, carry both chemical and structural information. Therefore by studying the temperature evolution of phonons, one can analyze the temperature-induced structural transformations and the effect of compositional variations on the coupling processes. Both IR and Raman spectroscopy are restricted to measurements of phonons with a wave vector k=0.[14]

IR spectroscopy involves an absorption process. Polychromatic IR radiation are fed onto a sample and the transition between molecular vibrational energy levels is measured.[14,30] Raman spectroscopy measures the frequency shift of inelastically scattered light produced by phonon excitations, where the scattered photon has a greater energy than the vibrational quantum energy. A part of its energy is lost to the atomic vibration and the rest is being scattered as a photon with lower energy.[5,30]

Although the Raman effect was discovered at the end of the 1920s, the Raman spectroscopy only became popular later, after the development of lasers, which permitted spectroscopic measurements of high resolution.[14] During the experiment, the laser irradiates the sample with monochromatic radiation. If the excitation is in the visible spectral region, the Raman scattered light will also be in the visible region. Two processes involving scattering of light take place: Rayleigh and Raman processes. During the Rayleigh process the light is elastically scattered and no energy is lost, while during a Raman process the scattered photons lose a part of their energy.[30] Raman scattering by atomic vibration starting from the ground vibrational state is called Stokes Raman scattering. If the incident photon interacts with a phonon from a vibrational excited state, an Anti-Stokes scattering takes place (Figure 17).[30]

In a solid not all vibrational modes are spectroscopically active. They can be IR-active, Raman-active or silent. In order to generate a Raman peak, the phonon must change the bond polarizability. These atomic vibrations are then called "Raman-active". In order to identify the Raman-active modes, the group theory delivers a set of selection rules based on symmetry operations.[14] A group-theory analysis will be performed in Chapter 4.4.

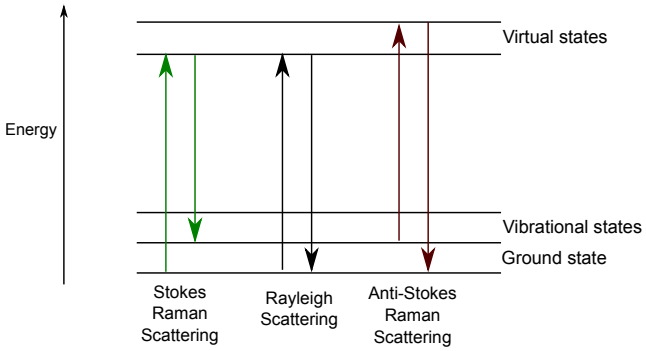

Figure 17: Rayleigh and Raman scattering

4.2 Experimental data collection

The measurements were carried out on pressed powder pellets. The $PbTiO_3$ powder with a purity of 99.9% was purchased from the American company Sigma-Aldrich. The solid solution (1-x)$PbTiO_3$-x$BiMg_{0.5}Ti_{0.5}O_3$ with x=0.20 was prepared by Prof. Jun Chen from the Department of Physical Chemistry, University of Science and Technology Beijing (China) after the conventional solid-state reaction method. Powders of $MgTiO_3$, PbO, TiO and Bi_2O_3 compounds were mixed together and ball milled in ethanol for 12 hours. This process was followed by a calcination at 850°C for 5 hours and another ball milling in ethanol for 12 hours. The powders were then uniaxially pressed into pellets with a diameter of 10mm and a thickness of 1mm. The pellets were hydrostatically compacted at 200MPa. The last step was the sintering of the pellets in a covered crucible at 1100°C for 2 hours.[25] The chemical composition of the pellets was verified by electron microprobe analysis (Cameca Microbeam SX100 with a wavelength-dispersive detector), averaging over 100 points.

The in-situ Raman spectroscopic experiments were conducted with a Horiba Jobin-Yvon T64000 triple-monochromator spectrometer coupled with an Olympus BX41 confocal microscope. The 514.5nm green line of an Ar^+ laser in backscattering geometry was used for the experiment. The laser was focused on the sample through a 50x LWD microscope objective. At room temperature spectra were collected from multiple points to check the repeatability of the data. No polarization, orientation, or spatial dependence of the Raman spectra was detected, indicating that the average linear crystallite size is much smaller than the diameter of the laser spot on the sample surface, which was $\sim 2\mu$m. The program used for data collection was LabSpec Spectroscopy Suite Software. The spectra were recorded on cooling between 870K and 100K every 10K with an accuracy of $\pm 0.1K$ in a Linkam THMS-E600 stage. The spectral resolution was 2cm^{-1}. For PT the acquisition was set for 10 accumulations with an exposure time of 10 seconds each. For PT-BMT the acquisition was set for 10 accumulations with an exposure time of 15 seconds each. The background noise was measured after every sample at the same objective-device distance as the sample, but aside of it.

4.3 Experimental data processing

In order to gain more information from the collected Raman spectra, such as: the peak position ω, the full width at half maximum (FWHM) of the modes and the normalized intensity, the data was processed with the program OriginPro 9.1 by performing the following steps:

1. The raw data collected with LabSpec was imported in OriginPro.

2. Baseline corrections were made by removing the instrumental background.

3. The Raman intensity was corrected using the Bose-Einstein factor

$$I_{reduced} = \frac{I_{measured}}{n(\omega, T) + 1}$$

where

$$n(\omega, T) = \frac{1}{e^{\frac{\hbar\omega}{k_B T}} - 1}$$

and $\hbar = 1.05457266x10^{-34}Js$ and $k_B = 1.380658x10^{-23}J/\mathrm{K}$.

4. The obtained intensity was divided by the accumulation time in order to express the intensity in counts per second.

5. The value of the intensity was normalised to [0,1].

6. The spectra were fitted with a pseudo-Voigt function, which is a weighted sum of Gaussian and Lorentzian functions:

$$y = y_0 + A[\mu\frac{2}{\pi}\frac{\omega}{4(x - x_c)^2 + \omega^2} + (1 - \mu)\frac{\sqrt{4ln2}}{\sqrt{\pi}\omega}e^{-\frac{4ln2}{\omega^2}(x-x_c)^2}] \tag{4.1}$$

where y_0 is the offset, x_c the center, A the area, ω the FWHM and μ the profile shape factor, with $\mu \in [0, 1]$.

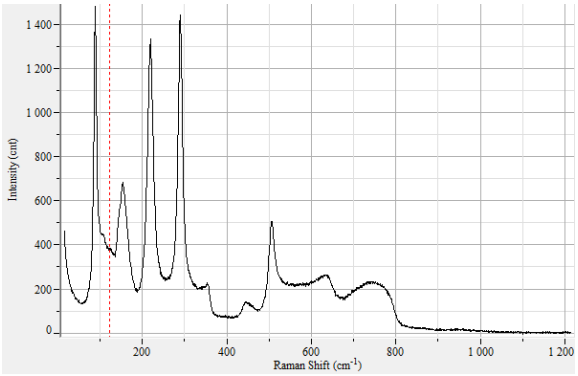

(a)

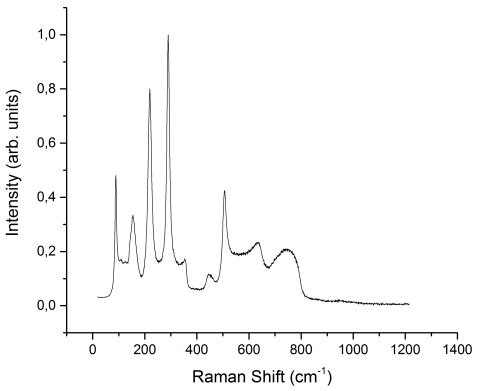

(b)

Figure 18: $PbTiO_3$ at room temperature (a) Raw data - capture from LabSpec (b) Data processed with OriginPro

4.4 Group-theory analysis

Group theory is a powerful method in the evaluation of vibrational spectra. Using group theory, one can anticipate if a vibrational mode is Raman- or IR-active based on the point group of the analyzed crystal.[2] For ferroic materials deviation of the predicted number of Raman-active modes can be indicative of local structural distortions, resulting in spatial regions of lower symmetry than the symmetry of the average structure, which are too small to be detected by standard diffraction methods. We will further analyze the character tables of $Pm\bar{3}m$ and $P4mm$, which are the space groups of PT and PT-BMT above and below the Curie temperature. The character tables deliver important information about particular point groups, such as the symmetry operations allowed and the number of the irreducible representations for a specific point group, described by the Mulliken's symbols. Following the Mulliken's symbols are described:[2]

A: Symmetric with respect to principal axis of symmetry (one dimensional representation)

B: Antisymmetric with respect to principal axis of symmetry (one dimensional representation)

E: Doubly degenerate, two dimensional irreducible representation

T: Triply degenerate, three dimensional irreducible representation

$\mathbf{X_1}$**:** symmetric with respect to a vertical mirror plane perpendicular to the principal axis

$\mathbf{X_2}$**:** anti-symmetric with respect to a vertical mirror plane perpendicular to the principal axis

$\mathbf{X_g}$**:** Symmetric with respect to a center of symmetry

$\mathbf{X_u}$**:** Antisymmetric with respect to a center of symmetry

The Bilbao Crystallographic Server `www.cryst.ehu.es`[15] was used to calculate the active Raman modes for PT and PT-BMT. All the pictures used in Chapter 4.4 are captures from the Bilbao Crystallographic Server.

O_h(m-3m)	#	1	4	2	3	2'	-1	-4	m	-3	m'	functions
Mult.	-	1	6	3	8	6	1	6	3	8	6	·
A_{1g}	Γ_1^+	1	1	1	1	1	1	1	1	1	1	$x^2+y^2+z^2$
A_{1u}	Γ_1^-	1	1	1	1	1	-1	-1	-1	-1	-1	·
A_{2g}	Γ_2^+	1	-1	1	1	-1	1	-1	1	1	-1	·
A_{2u}	Γ_2^-	1	-1	1	1	-1	-1	1	-1	-1	1	·
E_g	Γ_3^+	2	0	2	-1	0	2	0	2	-1	0	$(2z^2-x^2-y^2,x^2-y^2)$
E_u	Γ_3^-	2	0	2	-1	0	-2	0	-2	1	0	·
T_{2u}	Γ_5^-	3	-1	-1	0	1	-3	1	1	0	-1	·
T_{2g}	Γ_5^+	3	-1	-1	0	1	3	-1	-1	0	1	(xy,xz,yz)
T_{1u}	Γ_4^-	3	1	-1	0	-1	-3	-1	1	0	1	(x,y,z)
T_{1g}	Γ_4^+	3	1	-1	0	-1	3	1	-1	0	-1	(J_x,J_y,J_z)

(a)

Check	WP	Representative
☐	48n	x,y,z
☐	24m	x,x,z
☐	24l	1/2,y,z
☐	24k	0,y,z
☐	12j	1/2,y,y
☐	12i	0,y,y
☐	12h	x,1/2,0
☐	8g	x,x,x
☐	6f	x,1/2,1/2
☐	6e	x,0,0
☑	3d	1/2,0,0
☐	3c	0,1/2,1/2
☑	1b	1/2,1/2,1/2
☑	1a	0,0,0

(b)

Figure 19: (a) Character table for the space group $Pm\bar{3}m$ (b) The occupied Wyckoff positions (checked in) of PT and PT-BMT compounds with space group $Pm\bar{3}m$.[15]

For the space group Pm$\bar{3}$m the Wyckoff positions of PT and BMT are (Figure 19b):

PT:	Pb	1b	$(\frac{1}{2},\frac{1}{2},\frac{1}{2})$	**BMT**:	Bi	1b	$(\frac{1}{2},\frac{1}{2},\frac{1}{2})$
	Ti	1a	(0,0,0)		Mg, Ti	1a	(0,0,0)
	O	3d	$(\frac{1}{2},0,0)$		O	3d	$(\frac{1}{2},0,0)$

In the cubic phase there are 5 triply degenerate modes (Figure 20), which means that a total of 15 phonons is expected: 3 acoustic modes (1b: T_{1u}) and 12 optical phonons corresponding to the irreducible representations of the Pm$\bar{3}$m point group. Since, on one hand, the wavenumber is inversely proportional to the square root of the atomic mass and, on the other hand, the wavenumbers of the acoustic modes approaches zero at the center of the Brillouin zone, the acoustic T_{1u} is attributed to the heaviest Pb/Bi atoms at 1b, while the optical T_{1u} are attributed to Ti/Mg at 1a: T_{1u} and oxygen atoms at 3d: $2T_{1u}$+T_{2u}. The $3T_{1u}$ modes are IR-active and the T_{2u} mode is a silent mode (neither IR- nor Raman-active).[12]

WP	A_{1g}	A_{1u}	A_{2g}	A_{2u}	E_u	E_g	T_{2u}	T_{2g}	T_{1u}	T_{1g}	Modes
1a	·	·	·	·	·	·	·	·	1	·	Show
1b	·	·	·	·	·	·	·	·	1	·	Show
3d	·	·	·	·	·	·	1	·	2	·	Show

Figure 20: The mechanical representation of the Wyckoff positions for the space group $Pm\bar{3}m$[15]

Based on the selection rules for the Raman-active modes which can be seen in the "functions" column from the character table (Figure 19a), none of the modes in the paraelectric phase is expected to be Raman-active (Figure 21).

WP	A_{1g}	A_{1u}	A_{2g}	A_{2u}	E_u	E_g	T_{2u}	T_{2g}	T_{1u}	T_{1g}
1a	·	·	·	·	·	·	·	·	·	·
1b	·	·	·	·	·	·	·	·	·	·
3d	·	·	·	·	·	·	·	·	·	·

Figure 21: Raman active modes for the space group $Pm\bar{3}m$[15]

At the Curie temperature, the perovskite structure undergoes a phase transition and the point group changes to $P4mm$. The new Wyckoff positions are (Figure 22b):

PT: Pb 1a (0,0,z)
Ti 1b $(\frac{1}{2},\frac{1}{2},z)$
O1 1b $(\frac{1}{2},\frac{1}{2},z)$
O2 2c $(\frac{1}{2},0,z)$

BMT: Bi 1a (0,0,z)
Mg, Ti 1b $(\frac{1}{2},\frac{1}{2},z)$
O1 1b $(\frac{1}{2},\frac{1}{2},z)$
O2 2c $(\frac{1}{2},0,z)$

C_{4v}(4mm)	#	1	2	4	m_x	m_d	functions
Mult.	-	1	1	2	2	2	·
A_1	Γ_1	1	1	1	1	1	z,x^2+y^2,z^2
A_2	Γ_2	1	1	1	-1	-1	J_z
B_1	Γ_3	1	1	-1	1	-1	x^2-y^2
B_2	Γ_4	1	1	-1	-1	1	xy
E	Γ_5	2	-2	0	0	0	$(x,y),(xz,yz),(J_x,J_y)$

(a)

Check	WP	Representative
☐	8g	x,y,z
☐	4f	x,1/2,z
☐	4e	x,0,z
☐	4d	x,x,z
☑	2c	1/2,0,z
☑	1b	1/2,1/2,z
☑	1a	0,0,z

(b)

Figure 22: (a) Character table for the space group $P4mm$ (b) The Wyckoff positions of the atoms in the PT and PT-BMT structures for the space group $P4mm$.[15]

In the tetragonal phase the triply degenerate T_{1u} modes split into A_1+E modes (1a, 1b and 2c) and the T_{2u} mode splits into B_1+E modes (2c) (Figure 23). The A_1+E modes are further split into longitudinal (LO) and transverse (TO) modes because of long-range electrostatic forces in the ferroelectric phase.[12]

WP	A_1	A_2	B_1	B_2	E	Modes
1a	1	·	·	·	1	Show
1b	1	·	·	·	1	Show
2c	1	·	1	·	2	Show

Figure 23: The mechanical representation of the Wyckoff positions for the space group $P4mm$.[15]

For the space group $P4mm$ the total number of modes is:

$$\Gamma_{total} = A_1 + E + A_1 + E + A_1 + E + B_1 + E + A_1 + E = 4A_1 + B_1 + 5E,$$

from which

$$\Gamma_{ac} = A_1 + E = 3 \text{ phonons},$$

corresponding to the 1a position, are acoustic modes and the rest are optical modes. Because of the LO-TO splitting of the A_1 and E modes and based on the above-mentioned selection rules (Figure 22a), we are expecting a total of

$$\Gamma_{opt} = 3A_1(TO) + 3A_1(LO) + B_1 + 4E(TO) + 4E(LO) = 15 \text{ phonons}$$

to be Raman-active (Figure 24).

WP	A_1	A_2	B_1	B_2	E
1a	1	·	·	·	1
1b	1	·	·	·	1
2c	1	·	1	·	2

Figure 24: Raman active modes for the space group $P4mm$[15]

5 Results and discussion

The results of the measurements described in the previous chapter are presented and discussed in this chapter. The polycrystalline ceramic (1-x)$PbTiO_3$-x$BiMg_{0.5}Ti_{0.5}O_3$ has a morphotropic phase boundary at x=0.63, where the monoclinic and tetragonal phases coexist.[17] In this thesis we will analyze the compound with x=0.20, which is on the tetrahedral side (Figure 25), and compare it to pure $PbTiO_3$.

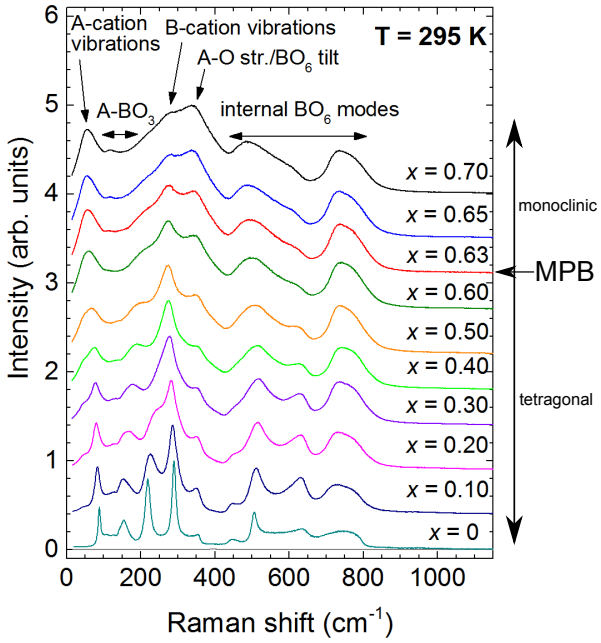

Figure 25: Raman spectra for compounds of the solid solution (1-x)$PbTiO_3$-x$BiMg_{0.5}Ti_{0.5}O_3$ with different amount of $BiMg_{0.5}Ti_{0.5}O_3$. The spectra were measured at room temperature. The peak assignment is after Datta[37] and Welsch.[32]

5.1 Temperature-dependent Raman spectra of 0.8PT-0.2BMT and PT

$PbTiO_3$ is cubic above the Curie temperature T_C=763K,[27] with the space group $Pm\bar{3}m$. The solid solution (1-x)$PbTiO_3$-x$BiMg_{0.5}Ti_{0.5}O_3$ with x=0.20 has the same symmetry of the paraelectic phase. The reported Curie temperature is ~810 K.[27] The ferroelectic phase of both pure PT and 0.8PT-0.2BMT has tetragonal symmetry with space group $P4mm$. Polarization measurements for (1-x)PT-xBMT with x between 0.56 and 0.66 revealed the existence of the depoling temperature T_{dep}, which is approximately 100K below T_C. The strong decrease in the spontaneous polarization suggests additional structural transformation on cooling, which should be of ferroelectric-antiferroelectric type. It should be noted that such a structural transformation has not been reported on the basis of Bragg diffraction analyzes, indicating that the atomic rearrangements may occur only on the mesoscopic length scale. Data for x=0.20 has not been reported, but one may assume that T_{dep} exists also for this compound. As seen in Chapter 4.4, there are 5 phonon modes in the paraelectric cubic phase: one triply degenerate acoustic mode, T_{1u}, and four triply degenerate optical modes: three polar T_{1u}

modes and one nonpolar T_{2u} mode. The lowest frequency T_{1u} is the soft mode.[9] Based on the selection rules for the space group $Pm\bar{3}m$ discussed above, no Raman-active modes should appear in this configuration. However, Raman scattering above the T_C can be noticed for both compounds (Figure 26 and 27), which is an evidence for local distortions in the paraelectric phase.[9]

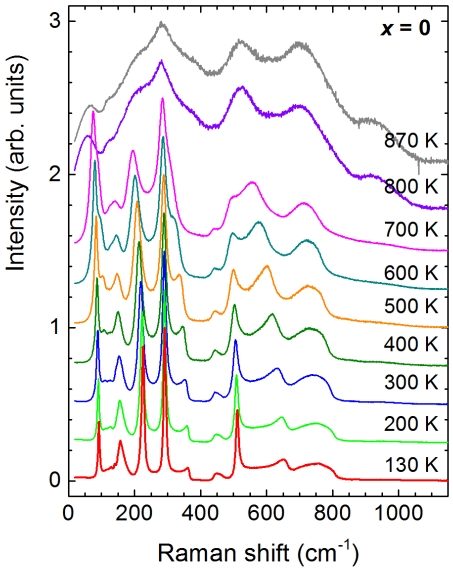

Figure 26: Raman spectra of $PbTiO_3$ measured at different temperatures. The spectra are normalized to the intensity of the strongest peak near 280cm^{-1} and vertically offset for clarity.

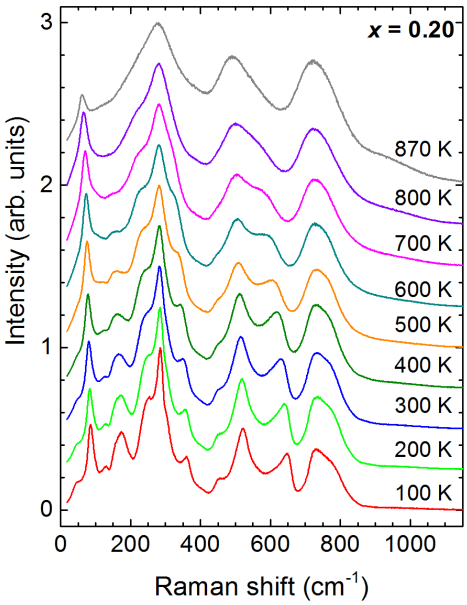

Figure 27: Raman spectra of PT-0.2BMT measured at different temperatures. The spectra are normalized to the intensity of the strongest peak near 280cm^{-1} and vertically offset for clarity.

At T_C both compounds undergo a first-order transition to a tetragonal structure: $P4mm$.[9] The triply degenerate modes are splitting in A_1, B_1 and E modes, as described in Chapter 4.4. The soft mode T_{1u} splits into A_1(1TO) and E(1TO).[10] The frequency of the soft mode decreases near the Curie temperature and stops at 55cm^{-1}.[9] This softening is caused by a change in the short-range interaction between Pb and O atoms along this bond.[7] The wavenumber of the optical phonon modes in $PbTiO_3$ and in (1-x)$PbTiO_3$-x$BiMg_{0.5}Ti_{0.5}O_3$ with x=0.20 measured at room temperature is given in Table 1. The observed peak positions in the spectra of the polycrystalline samples studied here are compared to existing literature.[8,10,26] The symmetry assignment is based on similarity in Raman peaks positions for our samples and those for single-crystal PT.[8] However, it should be emphasised that the vibrational states in polar crystals that are arbitrarily oriented to the direction of the incident photon are quasi-LO and quasi-TO phonons with mixed symmetry and wavenumbers depending on the angle between the phonon propagation and the crystallographic polar axis. This further complicates the application of symmetry analysis to Raman spectra of polycrystalline multidomain compounds, as the samples studied here. Nevertheless, in the text below we will refer to the observed peaks following the notation given in Table 1.

Phonon mode	Literature PT	Measured PT	Measured PT-BMT
E(1TO)	87.5	88.5	80
E(1LO)	128	125	124
A_1(1TO)	148.5	153	154
A_1(1LO)	194		
E(2TO)	218	218.5	241
B_1+E	287	290	283
A_1(2TO)	359.5	350	351
E(2LO)	440	447	452
A_1(2LO)	465		
E(3TO)	505	506	513
A_1(3TO)	647	627	636
E(3LO)	687	724	724
A_1(3LO)	795	770	711

Table 1: Observed peak positions (in cm^{-1}) in the Raman spectra of studied polycrystalline samples, compared with the reported phonon wavenumbers for $PbTiO_3$ single crystal.[8]

The behaviour of the peaks on cooling at 870K, 760K (T_C in PT), 750K (T_C in 0.8PT-0.2BMT), 300K, 130K (in PT) and 100K (in 0.8PT-0.2BMT) can be observed in Figure 28 and Figure 29.

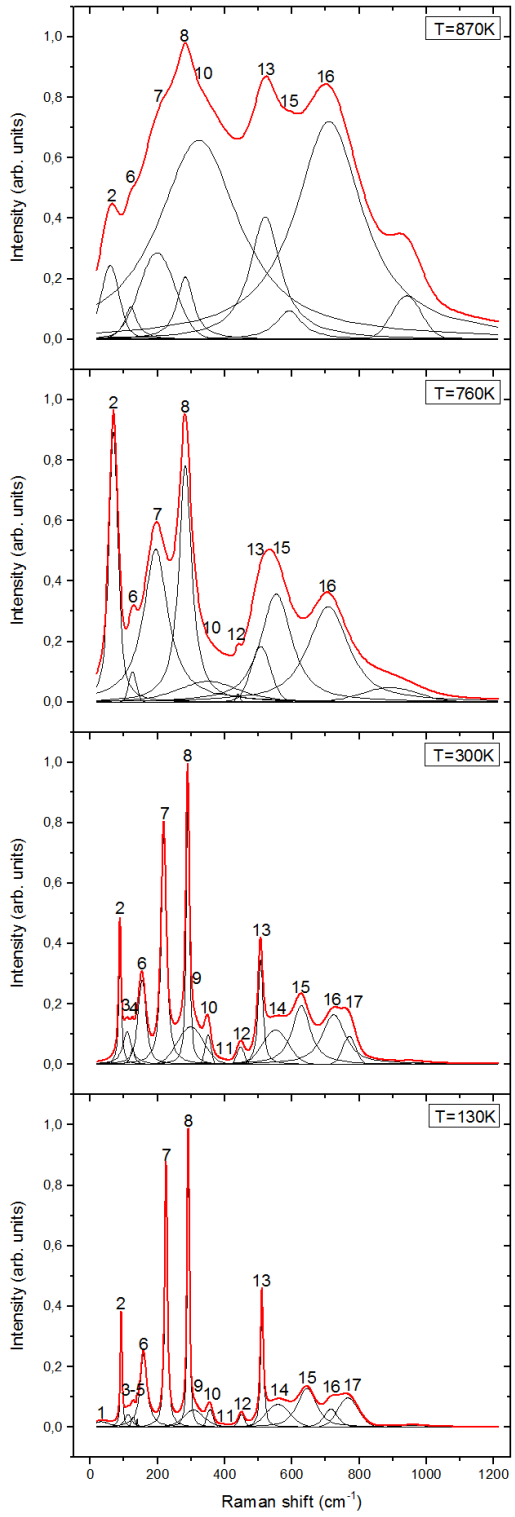

Figure 28: Behaviour of the peaks in PT on cooling

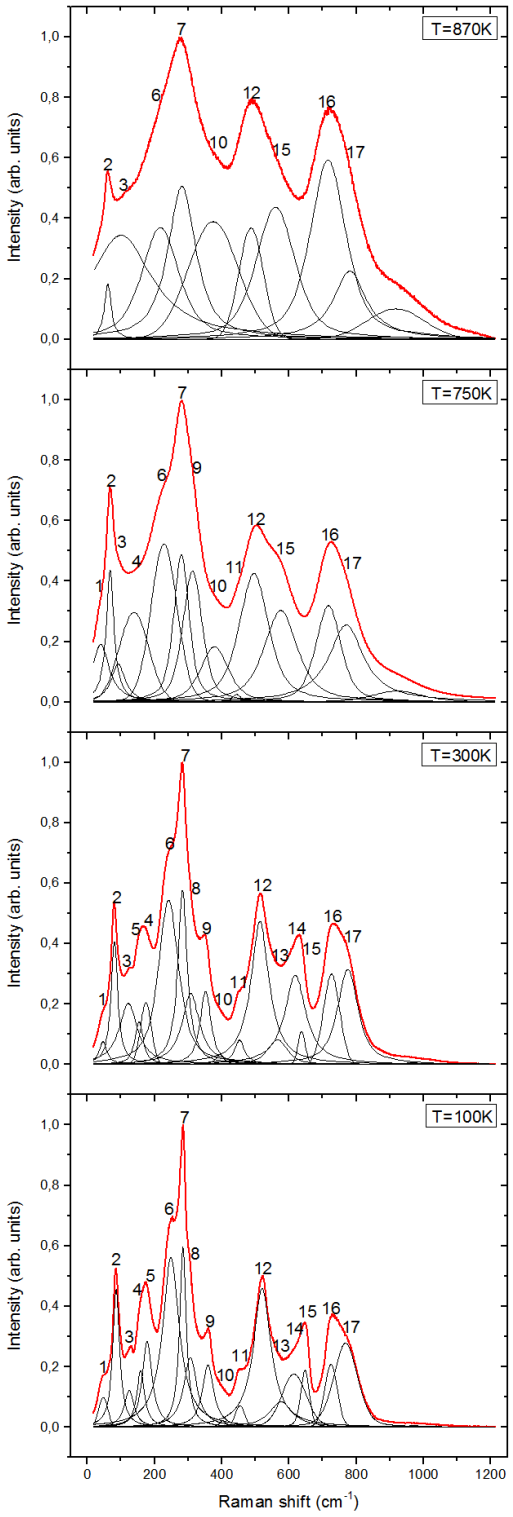

Figure 29: Behaviour of the peaks in 0.8PT-0.2BMT on cooling

5.2 Temperature trends of phonon wavenumbers, widths and intensities

In this thesis only the peaks generated by A-site and B-site cation vibrations and BO_3-A translations are discussed.

Vibrational modes in the frequency range of 20-90cm^{-1} are dominated by A-site cation vibrations. Vibrational modes in the frequency range of 90-200cm^{-1} are dominated by BO_6 vibrations against A-cation vibrations. Vibrational modes in the frequency range of 200-300cm^{-1} are dominated by B-site cation vibrations.[11] The peaks observed in our Raman spectra are described in Figure 30.

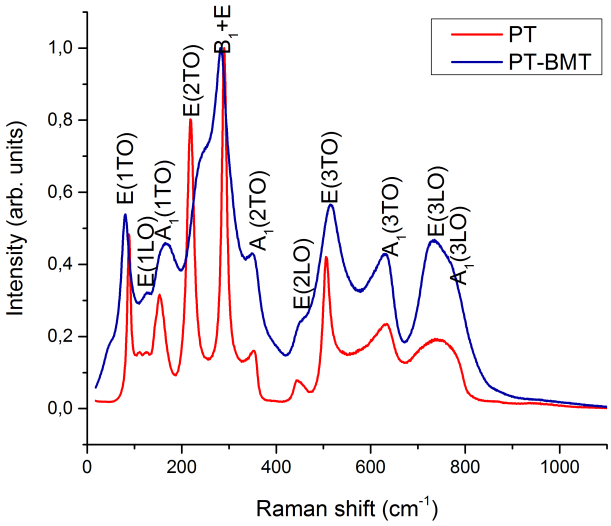

Figure 30: Raman spectra of PT and 0.8PT-0.20BMT measured at room temperature. Mode symmetry assignment of the observed peaks is according to data given in Table 1.[8]

Raman scattering between 20-90cm^{-1}

Peak 2 (80cm^{-1}) in 0.8PT-0.2BMT and peak 2 (88cm^{-1}) in PT are generated by the E(1TO) phonon mode, which involves mainly A-site cation vibrations.[8] The behaviour of ω, FWHM and the normalized integrated intensity of the E(1TO) phonon mode on heating together with the Lorentzian contributions for peak 2 can be seen in Figure 31a.

In PT the phonon mode E(1TO) exhibits a classical soft-mode behaviour at the Curie temperature. The soft mode reaches its minimum value (55cm^{-1}) at 780K. At this point peak 2 also reaches its FWHM maximum value and the highest intensity.

In 0.8PT-0.2BMT ω_2 decreases gradually on heating up to 870K. At T_C a maximum point in the FWHM can be observed. In both compounds peak 2 exists above the Curie temperature, which indicates ionic disorder in the lattice.[11] In 0.8PT-0.2BMT peak 2 could be fitted using mainly Gaussian functions, whereas in PT a combination of Gaussian and Lorentzian functions had to be used, especially at high temperatures. The softening of the phonon mode E(1TO) around T_C drives a displacive phase transition.[8]

Peak 1 (44cm^{-1}) (Figure 31b) exists only in the solid solution 0.8PT-0.2BMT and could be related to a different structural state of the A-site cations.[38] The behaviour of its frequency

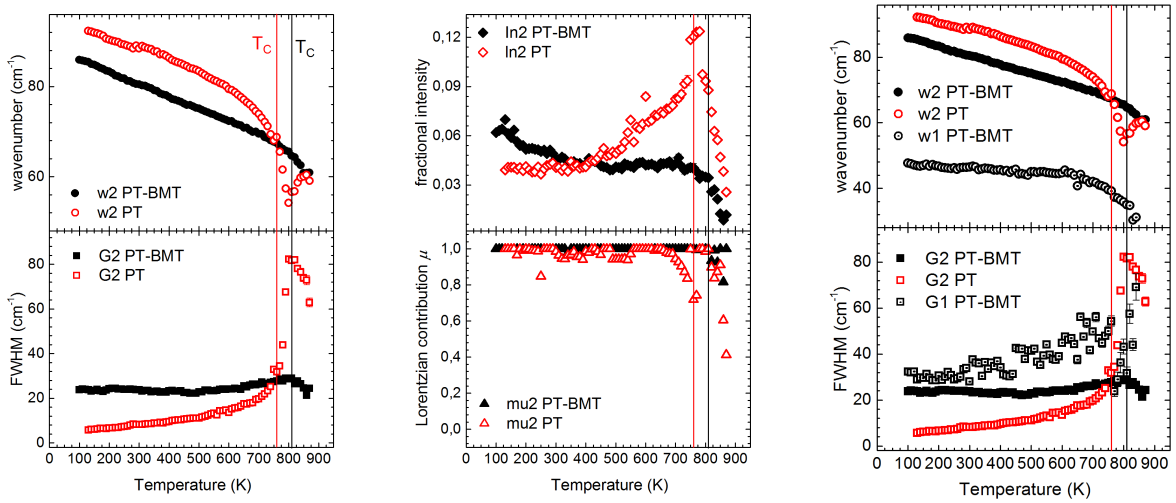

(a) (b)

Figure 31: (a) Peak 2 in PT and 0.8PT-0.2BMT. (b) Peak 1 in 0.8PT-0.2BMT and peak 2 in PT and 0.8PT-0.2BMT

on heating is similar to the one of peak 2 from the same compound. A minimum in the normalized splitting of peak 1 and 2 can be observed around 600K.

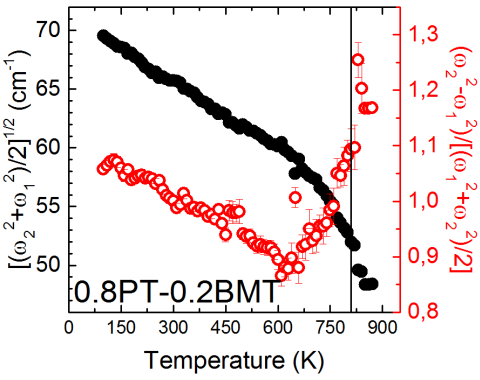

Figure 32: The average squared wavenumber and the normalized splitting of peak 1 and peak 2 in 0.8PT-0.2BMT

Raman scattering between 90-200 cm^{-1}

The E(1LO) phonon mode is represented by peak 3 (125cm^{-1}) in PT and peak 3 (124cm^{-1}) in 0.8PT-0.2BMT.[8] The peaks have the same origin in both compounds, being generated by BO_3-A translations and BO_3 vibrations against A-site cations vibrations.[11]

In 0.8PT-0.2BMT we can observe a softening of the phonon mode near the Curie temperature of PT, as its frequency reaches the minimum value 92cm^{-1} at T_C=750K. In PT ω_3 decreases continuously on heating and the peak vanishes at the transition temperature.
Both peaks have similar fractional intensities and low values at FWHM before the transition temperature. Above $T_{C(PT)}$ we can observe a high jump in the intensity and FWHM for peak 3 in 0.8PT-0.2BMT. The behaviour of ω, FWHM and the normalized integrated intensity of the

phonon mode E(1LO) on heating together with the Lorentzian contributions for peak 3 can be seen in Figure 33. Both peaks were fitted using a combination of Gaussian and Lorentzian functions.

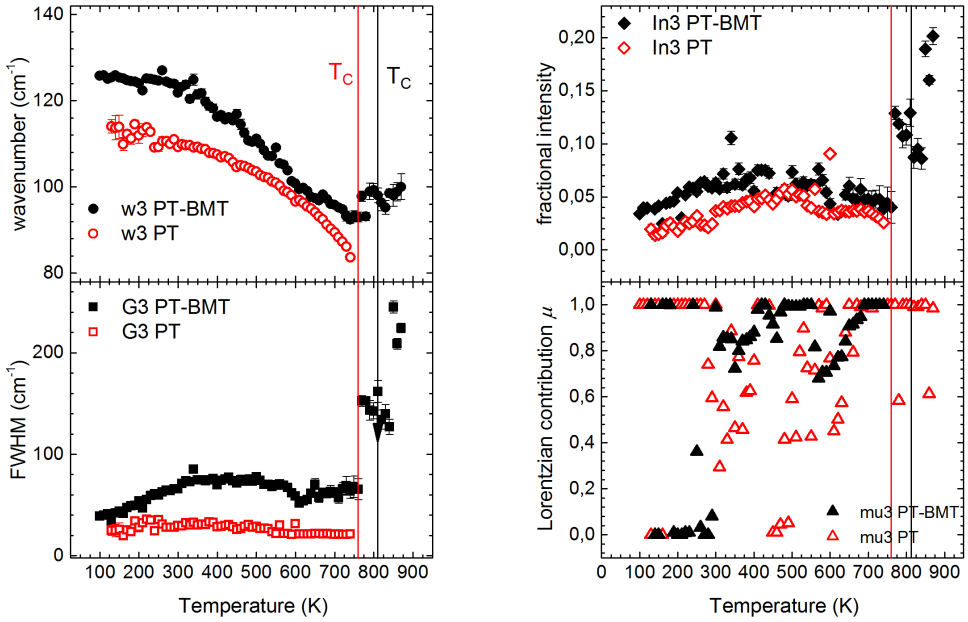

Figure 33: Peak 3 in PT and 0.8PT-0.2BMT

The phonon mode A_1(1TO) splits into two peaks in 0.8PT-0.2BMT (peak 4 (154cm^{-1}) and peak 5 (173cm^{-1})) and into three components in PT (peak 4 (125cm^{-1}), peak 6 (153cm^{-1}) and peak 5 (138cm^{-1}), which exists only below 200K and will not be discussed here).[8] A_1(1TO) is also generated by BO_3-A translations.

In PT we can observe a softening in the frequency of peak 6 near T_C. Peak 4 does not exhibit a significant decrease in the frequency between 130K and 760K. At the transition temperature peak 4 and peak 6 merge and become one peak.

In 0.8PT-0.2BMT peak 5 appears to be insensitive to changes in the temperature and disappears at 600K, whereas peak 4 exhibits an almost identical behaviour to peak 6 in PT up to the transition temperature, where it disappears. At $T_{C(PT)}$ peak 4 (0.8PT-0.2BMT) reaches its FWHM maximum value and the highest intensity, while peak 6 (PT) reaches its minimum in both cases. The behaviour of ω, FWHM and the normalized integrated intensity of the phonon mode A_1(1TO) on heating together with the Lorentzian contributions for peak 3 can be seen in Figure 34. All four peaks were fitted using a combination of Gaussian and Lorentzian functions.

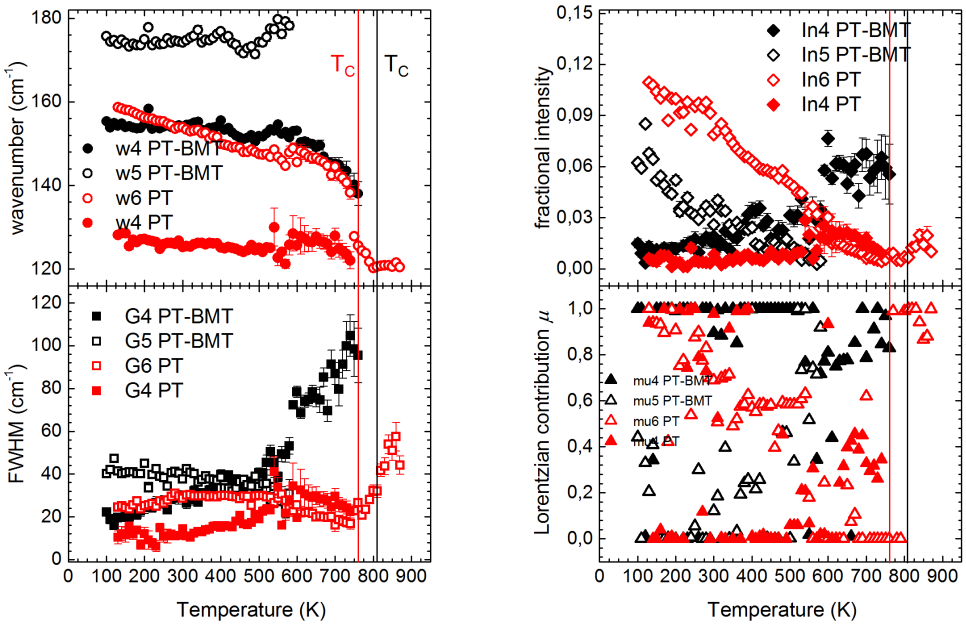

Figure 34: Peak 4 and peak 6 in PT and peak 4 and peak 5 in 0.8PT-0.2BMT

Raman scattering between 200-300 cm^{-1}

The phonon modes E(2TO) and B_1+E are generated by B-site cation vibrations. The phonon mode E(2TO) is represented by peak 6 (241cm^{-1}) in 0.8PT-0.2BMT and peak 7 (218cm^{-1}) in PT and the phonon mode B_1+E is represented by peak 7 (283cm^{-1}) in 0.8PT-0.2BMT and peak 8 (290cm^{-1}) and PT[8] (Figure 35).

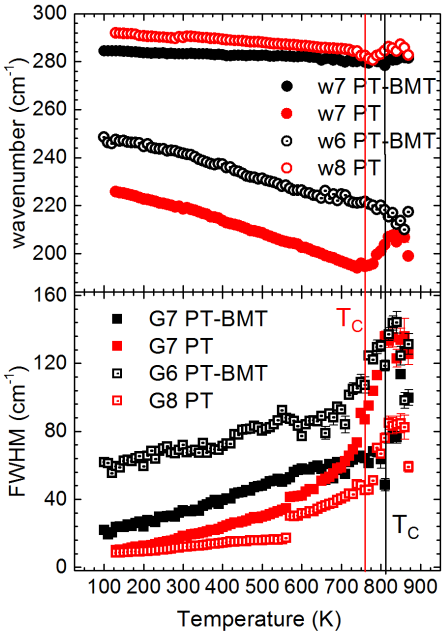

Figure 35: The phonon modes E(2TO) and B_1+E in PT and 0.8PT-0.2BMT

Peak 6 and peak 7

In PT ω_7 exhibits a minimum equal to 50cm^{-1} at T_C. Raman scattering can be observed above T_C (Figure 36). In 0.8PT-0.2BMT ω_6 decreases gradually with no remarkable changes at the transition temperature. Both peaks have exponentially increasing values of the FWHM on heating above T_C. The fractional intensity of peak 7 increases moderately on heating and drops in value after T_C. The fractional intensity of peak 6 varies with the temperature, with two local minima at 370K and 700K and a local maximum at 560K. Peak 6 was fitted using mainly Gaussian functions. For peak 7 a combination of Gaussian and Lorentzian functions had to be used.

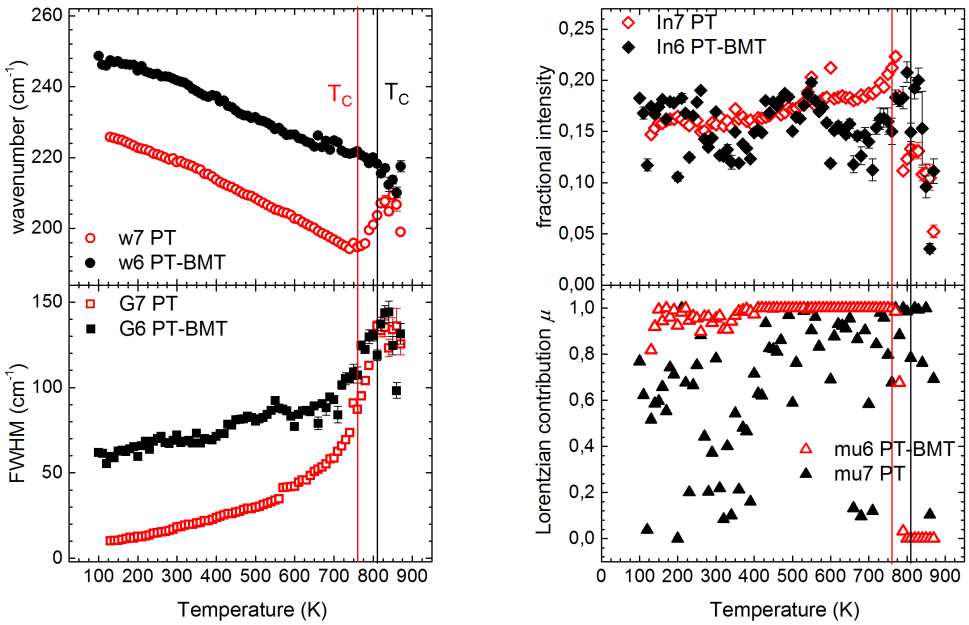

Figure 36: Peak 7 and peak 6 in PT and 0.8PT-0.2BMT

Peak 7 and peak 8

Minimum values near the Curie temperature can be observed in both components (Figure 37). In PT the frequency of the phonon mode decreases constantly to T_C, where it drops abruptly to 181cm^{-1}. In 0.8PT-0.2BMT a mild softening of the phonon mode can be noticed around 800K, with Raman scattering being present above the transition temperature in both cases. Both peaks have increasing values of the FWHM on heating. At 600K peak 7 exhibits a local maximum in the fractional intensity, while peak 8 makes a jump from 0.05 to 0.18. After T_C the fractional intensity of peak 7 is increasing, while the intensity of peak 8 is dropping. Peak 7 was fitted using a combination of Gaussian and Lorentzian functions at low temperatures and Lorentzian functions at high temperatures, whereas Gaussian functions at low temperatures and a combination of the two functions at high temperatures were used for peak 8.

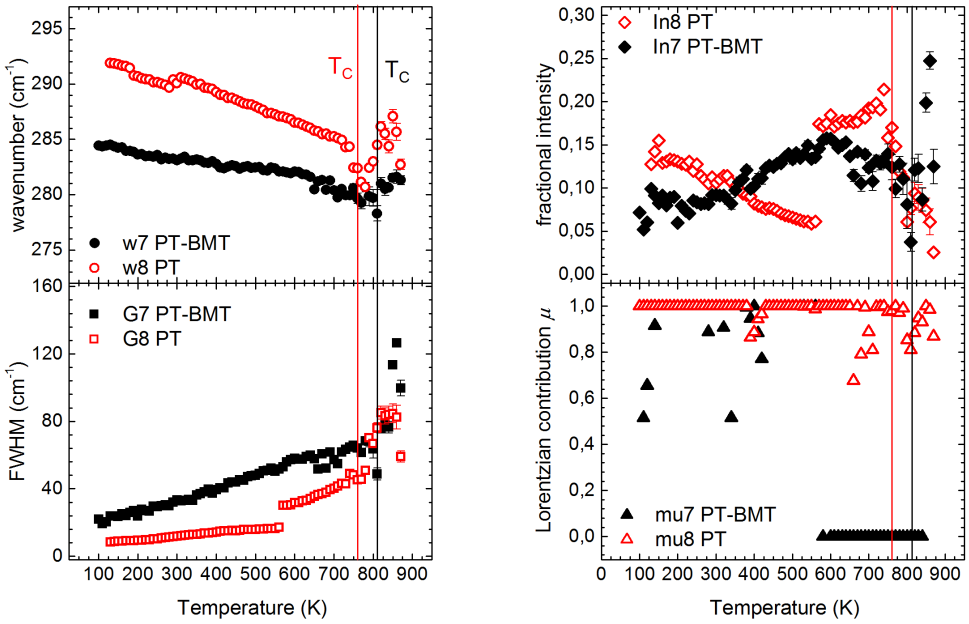

Figure 37: Peak 8 and peak 7 in PT and 0.8PT-0.2BMT

In PT a minimum in the average squared wavenumber and a maximum in the normalized splitting can be observed around 750K (Figure 38a). In 0.8PT-0.2BMT the average squared wavenumber decreases constantly on heating to 870K while the normalized splitting increases gradually up to the transition temperature, where an increase in the slope can be noticed. (Figure 38b)

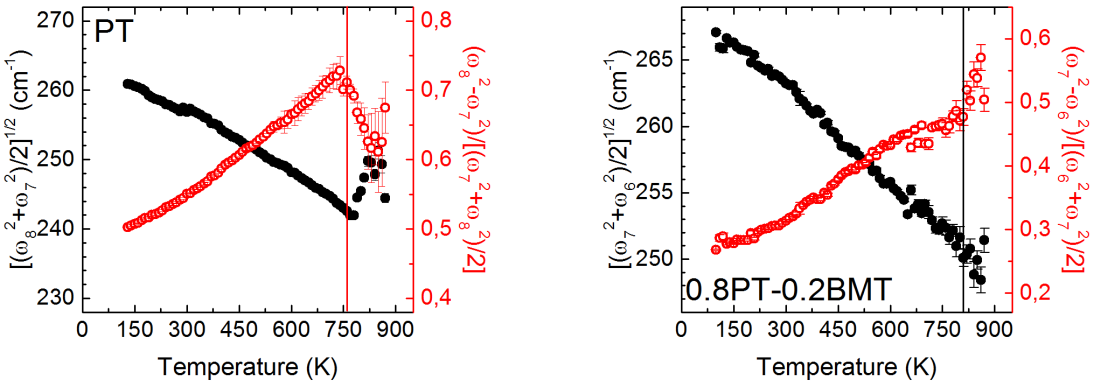

(a) (b)

Figure 38: The average squared wavenumber and the normalized splitting of (a) peak 7 and peak 8 in PT and (b) peak 6 and peak 7 in 0.8PT-0.2BMT

6 Conclusions

In this thesis the solid solution (1-x)$PbTiO_3$-x$BiMg_{0.5}Ti_{0.5}O_3$ with x=0.20 and pure $PbTiO_3$ were analyzed by Raman spectroscopy on cooling from 870K to 100K.

The comparison of the Raman spectra of the two compounds revealed that at high temperatures the spectra look similar, while at lower temperatures the peaks in 0.8PT-0.2BMT are broader than in PT. This broadening may be related to the presence of Bi and Mg ions in the lattice.[36] The addition of BMT in PT gives rise to local structural disorder and increases the off-center displacements of the A-site and B-site cations.[38] Anomalies in the temperature trends for the phonon modes in 0.8PT-0.2BMT indicate additional structural transformations below T_C, which might be related to depoling processes.

Although the Raman selection rules forbid it, we can observe Raman-active modes above the Curie temperature, in the paraelectric cubic phase, in both samples. This means that the A and B cations are locally displaced from their centrosymmetric positions above the transition temperature, which is an indicator for order-disorder phenomena.[5] Below T_C, in the tetragonal ferroelectric phase, the compounds seem to obey the selection rules and we can identify almost all phonon modes observed in single crystal PT.[8]

We can also notice a softening of the phonon modes around 80cm^{-1}, 125cm^{-1}, 153cm^{-1} and 290cm^{-1}. Compared to the softening of the phonon modes in 0.8PT-0.2BMT, where the wavenumber decreases gradually, in PT the minimum value is reached abruptly, with a drop in the wavenumber. The softening of the phonon mode generated by the A-cation and A-BO_3 translations at 88 cm^{-1}, 121cm^{-1} and 153cm^{-1} near T_C is responsible for the ferroelectric phase transition in PT and 0.8PT-0.2BMT.[8]

In order to understand the impact of adding $BiMg_{0.5}Ti_{0.5}O_3$ to pure $PbTiO_3$ and the behaviour of the resulting solid solution at the morphotropic phase boundary, further studies for different values of x should be conducted.

References

[1] The Editors of Encyclopaedia Britannica. Ferroelectricity. `https://www.britannica.com/science/ferroelectricity`.

[2] D. Tuschel. Practical group theory and raman spectroscopy, part I: Normal vibrational modes. `http://www.horiba.com/fileadmin/uploads/Scientific/Documents/Raman/Specy_Workbench-DT-Practical_Group_Theory__Raman_Spectroscopy-part_1.pdf`.

[3] B. Jaffe. *Piezoelectric Ceramics*. Academic Press, ISBN 978-0124332614, (1971).

[4] A. P. Fleury. The effects of soft modes on the structure and properties of materials. *Annual Review of Materials Science*, 6(1):157–180, (1976).

[5] M. E. Lines and A. M. Glass. *Principles and Applications of Ferroelectrics and Related Materials*. Oxford University Press Inc., ISBN 978-0198507789, (1977).

[6] J. M. Herbert. *Ferroelectric Transducers and Sensors*. Gordon and Breach, Science Publishers, Inc., ISBN 978-0677059108, (1982).

[7] M. Fontana, H. Idrissi, E. Kugel, and K. Wojcik. Raman spectrum in $PbTiO_3$ re-examined: dynamics of the soft phonon and the central peak. *Journal of Physics: Condensed Matter*, 3(44):8695, (1991).

[8] C. M. Foster, Z. Li, M. Grimsditch, S. Chan, and D. J. Lam. Anharmonicity of the lowest-frequency a1(to) phonon in pbtio3. *Phys Rev B Condens Matter*, 48:10160–10167, (1993).

[9] B. Ravel, N. Sicron, Y. Yacoby, E. A. Stern, F. Dogan, and J. J. Rehr. Order-disorder behavior in the phase transition of $PbTiO_3$. 164:265–277, (1995).

[10] L. Sun, Y. Chen, and D. Ding. Phonon-mode hardening in epitaxial $PbTiO_3$ ferroelectric thin films. *Phys. Rev. B*, 55:12218–12222, (1997).

[11] E. Husson. Raman spectroscopy applied to the study of phase transitions. *Key Eng. Mater*, 155-156:1, (1998).

[12] Yu. I. Yuzyuk, R. Farhi, V. L. Lorman, L. M. Rabkin, L. A. Sapozhnikov, E. V. Sviridov, and I. N. Zakharchenko. A comparative raman study of ferroelectric PbTiO3 single crystal and thin film prepared on mgo substrate. *Journal of Applied Physics*, 84(1):452–457, (1998).

[13] J. H. Simmons and K. S. Potter. *Optical Materials*. Academic Press, ISBN 978-0126441406, (2000).

[14] M. Dove. *Structure and Dynamics: An Atomic View of Materials*. Oxford University Press Inc., ISBN 978-0198506782, (2002).

[15] E. Kroumova, M. I. Aroyo, J. M. Perez-Mato, A. Kirov, C. Capillas, S. Ivantchev, and H. Wondratschek. Bilbao crystallographic server: useful databases and tools for phase-transition studies, (2003). Phase Transit. 76, 155.

[16] K. Kao. *Dielectric Phenomena in Solids*. Academic Press, ISBN 978-0080470160, (2004).

[17] C. A. Randall, R. Eitel, B. Jones, T. R. Shrout, D. I. Woodward, and I. M. Reaney. Investigation of a high tc piezoelectric system: (1-x)Bi(Mg1/2Ti1/2)O3-(x)PbTiO3. *Journal of Applied Physics*, 95(7):3633–3639, (2004).

[18] A. J. Bell. Factors influencing the piezoelectric behaviour of pzt and other morphotropic phase boundary ferroelectrics. *Journal of Materials Science*, 41(1):13–25, (2006).

[19] D. I. Bilc and D. J. Singh. Frustration of tilts and a-site driven ferroelectricity in $KNbO_3$-$LiNbO_3$ alloys. *Phys. Rev. Lett.*, 96:147602, (2006).

[20] R. Blinc. Order and disorder in perovskites and relaxor ferroelectrics. In *Ferro- and Antiferroelectricity*, volume 124 of *Structure and Bonding*, pages 51–67. Springer Verlag, (2007).

[21] P. Chandra and P. B. Littlewood. A landau primer for ferroelectrics. In *Physics of Ferroelectrics: A Modern Perspective*, volume 105 of *Topics in Applied Physics*, pages 69–116. Springer Verlag, (2007).

[22] K. M. Rabe and P. Ghosez. First-principles studies of ferroelectric oxides. In *Physics of Ferroelectrics: A Modern Perspective*, volume 105 of *Topics in Applied Physics*, pages 117–174. Springer Verlag, (2007).

[23] M. Ahart, M. Somayazulu, R. E. Cohen, P. Ganesh, P. Dera, H. Mao, R. Hemley, Y. Ren, P. Liermann, and Z. Wu. Origin of morphotropic phase boundaries in ferroelectrics. *Nature*, (451):545–548, (2008).

[24] W. D. Callister and D. G. Rethwisch. *Materials Science and Engineering: An Introduction.* John Wiley and Sons., ISBN 978-0470419977, (2009).

[25] J. Chen, X. Tan, W. Jo, and J. Roedel. Temperature dependence of piezoelectric properties of high-TC Bi(Mg1/2Ti1/2)O3-PbTiO3. *Journal of Applied Physics*, 106(3):034109, (2009).

[26] H. Deng, Y. Qiu, and S. Yang. General surfactant-free synthesis of $MTiO_3$ (M = Ba, Sr, Pb) perovskite nanostrips. *J. Mater. Chem.*, 19:976–982, (2009).

[27] K. Uchino. *Ferroelectric Devices. Second edition.* CRC Press, ISBN 978-1439803752, (2009).

[28] D. Damjanovic. A morphotropic phase boundary system basedon polarization rotation and polarization extension. *Applied Physics Letters*, 97(6), (2010).

[29] A-B. M. A. Ibrahim, R. Murgan, M. K. A. Rahman, and J. Osman. Morphotropic phase boundary in ferroelectric materials. *Ferroelectrics - Physical Effects*, (2011). Chapter 1.

[30] P. J. Larkin. *Infrared and Raman Spectroscopy. Principles and Spectral Interpretation.* Elsevier, ISBN 978-0123869845, (2011).

[31] R. Lopez-Juarez, F. Gonzalez, and M-E. Villafuerte-Castrejon. Lead-free ferroelectric ceramics with perovskite structure. In *Ferroelectrics - Material Aspects*, (2011). Chapter 15.

[32] A. M. Welsch, B. J. Maier, B. Mihailova, R. J. Angel, J. Zhao, C. Paulmann, J. M. Engel, M. Gospodinov, V. Marinova, and U. Bismayer. Transformation processes in relaxor ferroelectric PbSc0.5Ta0.5O3 heavily doped with Nb and Sn. *Zeitschrift fur Kristallographie - Crystalline Materials*, 226, (2011).

[33] T. Takenaka. Lead-free piezoelectric ceramics. In *Handbook of Advanced Ceramics: Materials, Applications, Processing and Properties*, pages 429–444. Elsevier, (2013).

[34] V. Fridkin and S. Ducharme. *Ferroelectricity at the Nanoscale. Basics and Applications.* Springer Verlag, ISBN 978-3642410062, (2014).

[35] J. Guyonnet. *Ferroelectric Domain Walls. Statics, Dynamics, and Functionalities Revealed by Atomic Force Microscopy.* Springer Theses, ISBN 978-3319057491, (2014).

[36] M. Polomska, Z. Hilczer, and J. Wolak. Xrd and raman spectroscopy studies of (bi1-xlaxfeo3)0.5(pbtio3)0.5 solid solution. *Phase Transitions*, 87:909–921, (2014).

[37] K. Datta, A. Richter, M. Göbbels, R. B. Neder, and B. Mihailova. Mesoscopic-scale structure and dynamics near the morphotropic phase boundary of (1-x)PbTiO3-xBiScO3. *Physical Review B*, 92, (2015).

[38] K. Datta, R. B. Neder, J. Chen, J. C. Neuefeind, and B. Mihailova. Atomic-level structural correlations at the morphotropic phase boundary of a ferroelectric solid solution: xBiMg1/2Ti1/2O3- (1-x)PbTiO3. *submitted*, (2016).

[39] R. J. D. Tilley. *Perovskites: Structure-Property Relationships.* John Wiley and Sons, ISBN 978-1118935668, (2016).

A PT-BMT-Peaks

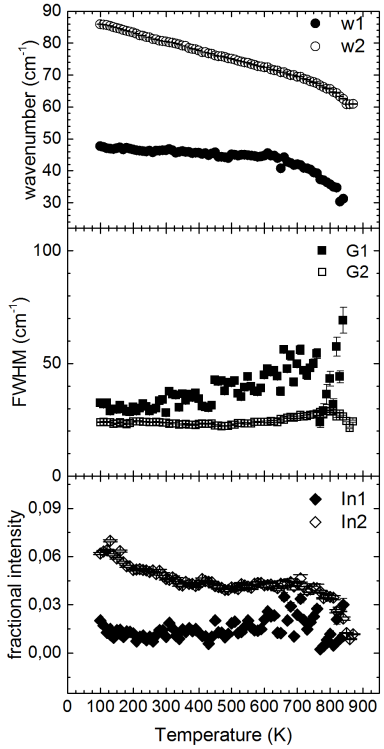

PTBMT-Peak 1 + 2

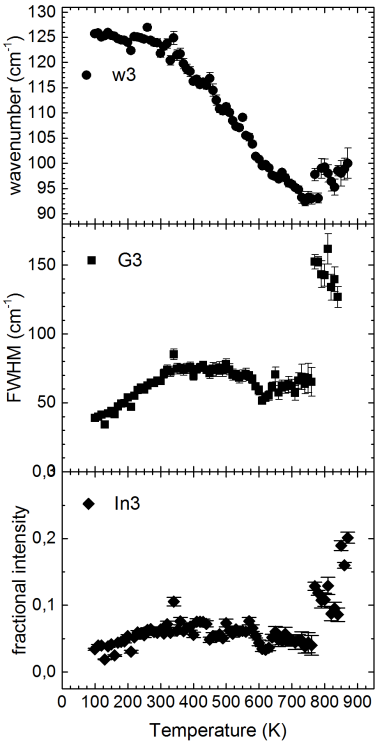

PTBMT-Peak 3

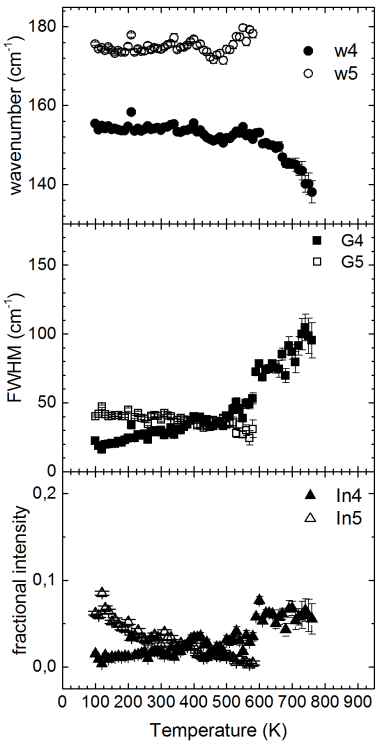

PTBMT-Peak 4 + 5

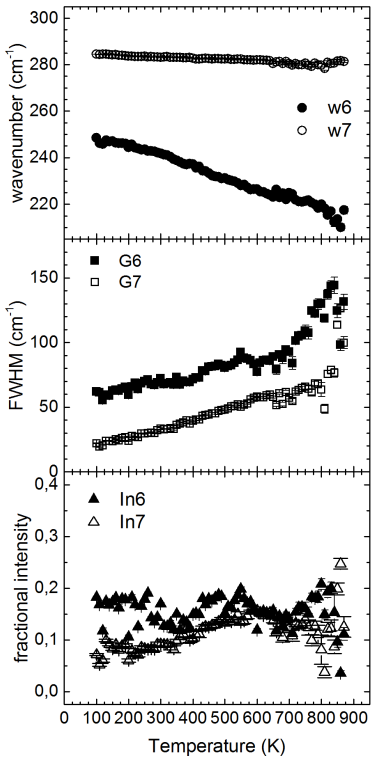

PTBMT-Peak 6 + 7

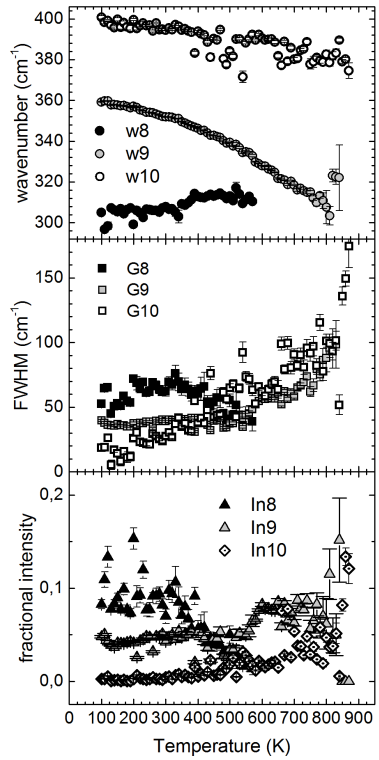

PTBMT-Peak 8 + 9 + 10

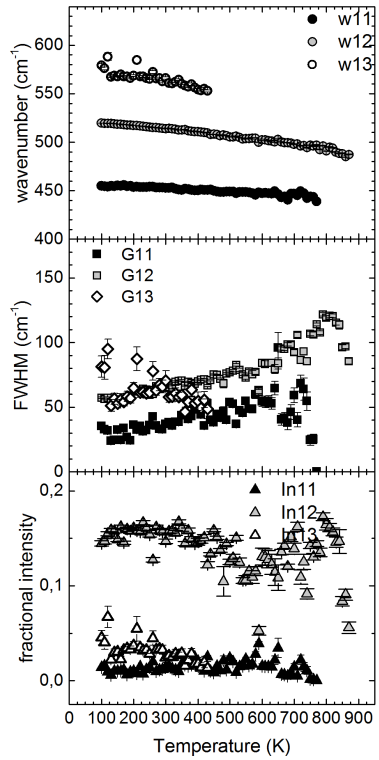

PTBMT-Peak 11 + 12 + 13

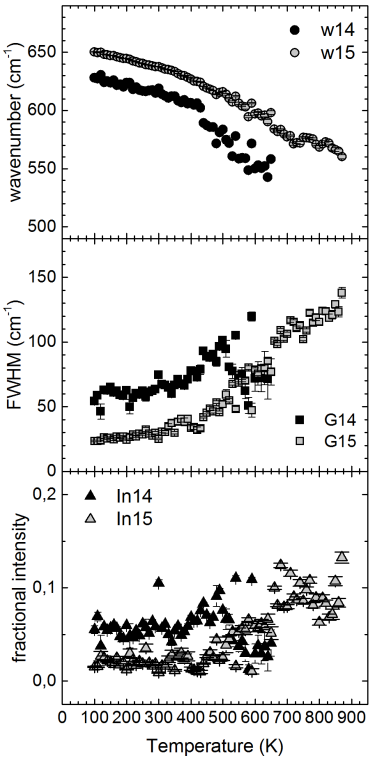

PTBMT-Peak 14 + 15

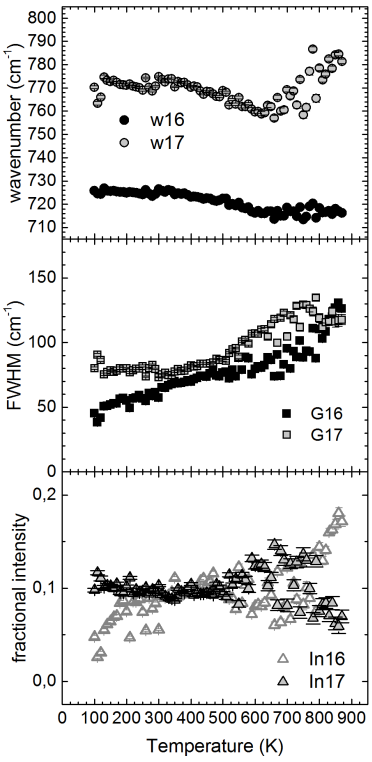

PTBMT-Peak 16 + 17

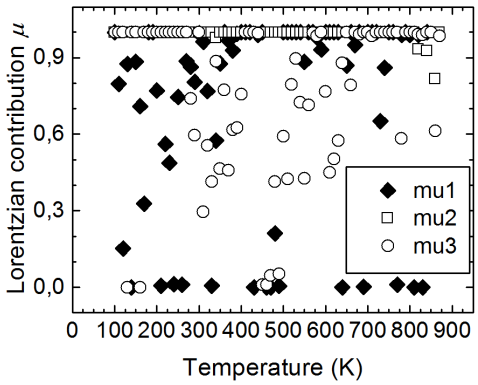

PTBMT-P1-P2-P3 Lorentzian contribution

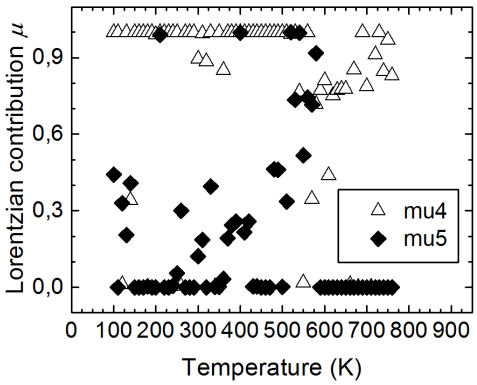

PTBMT-P4-P5 Lorentzian contribution

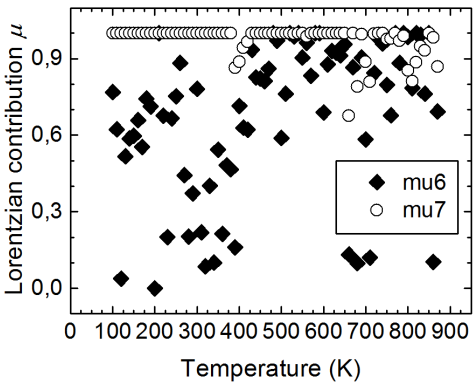

PTBMT-P6-P7 Lorentzian contribution

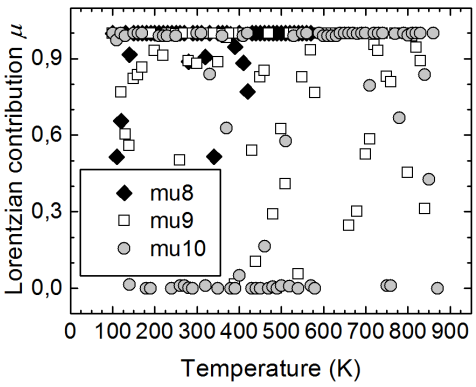

PTBMT-P8-P9-P10 Lorentzian contribution

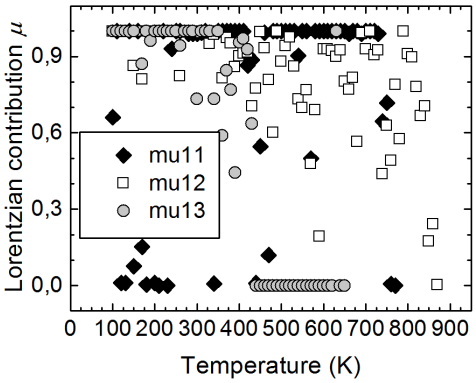

PTBMT-P11-P12-P13 Lorentzian contribution

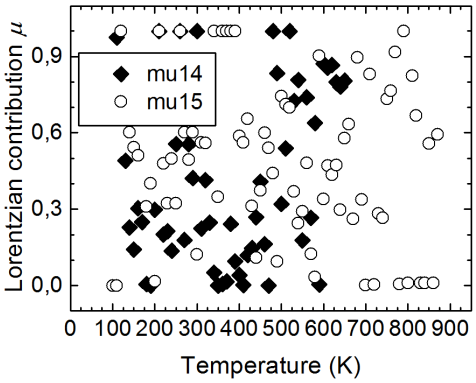

PTBMT-P14-P15 Lorentzian contribution

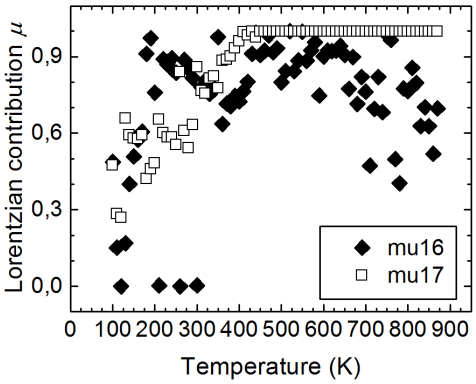

PTBMT-P16-P17 Lorentzian contribution

B PT-Peaks

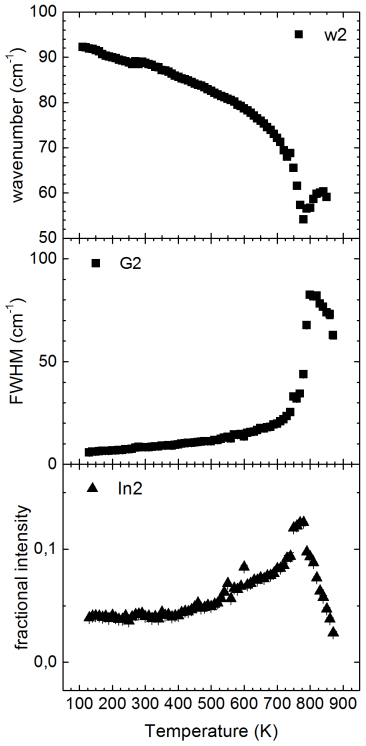

PT-P2

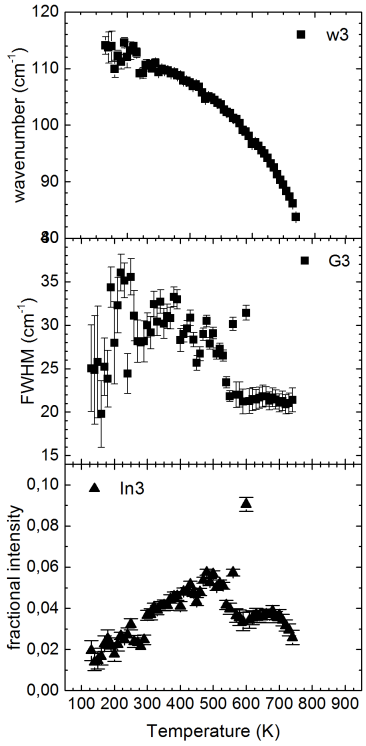

PT-P3

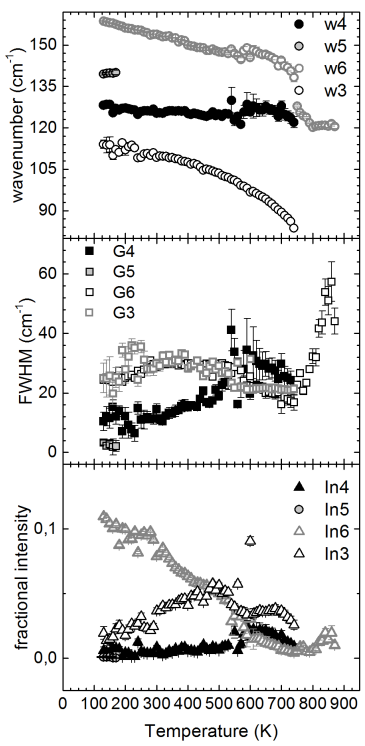

PT-P4-P5-P6

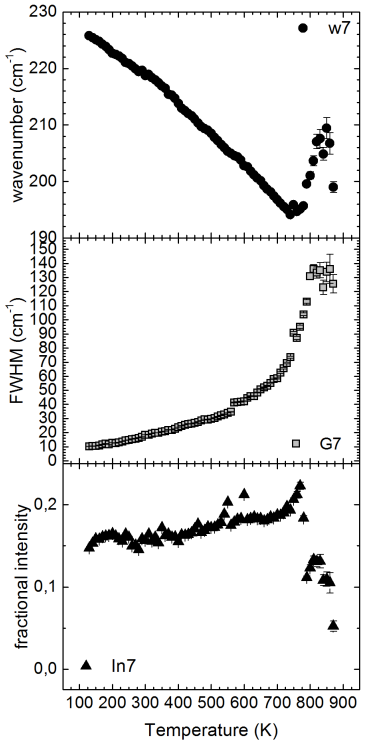

PT-P7

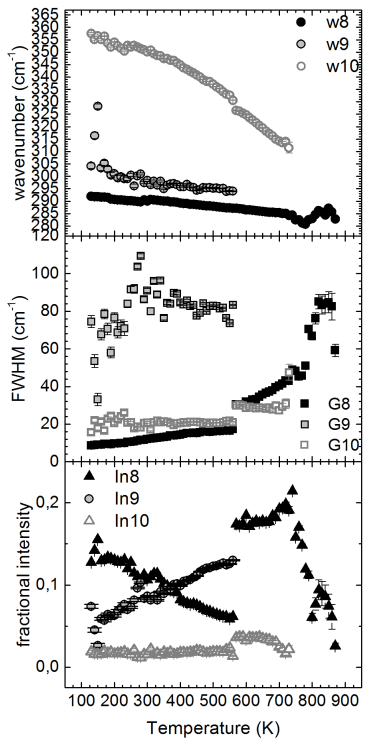

PT-P8-P9-P10

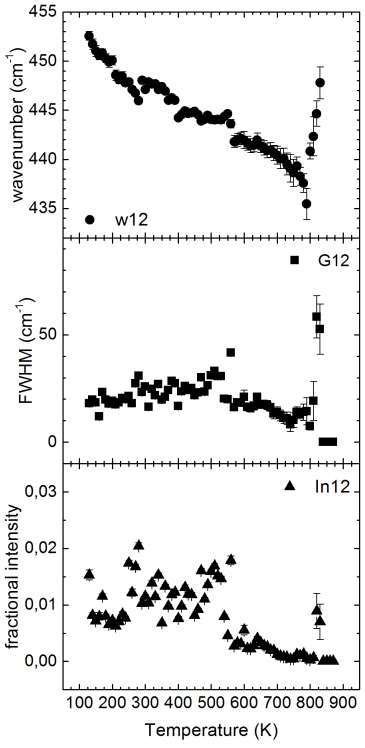

PT-P12

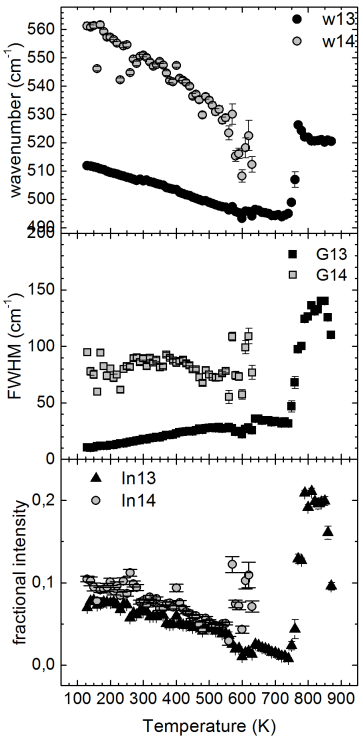

PT-P13-P14

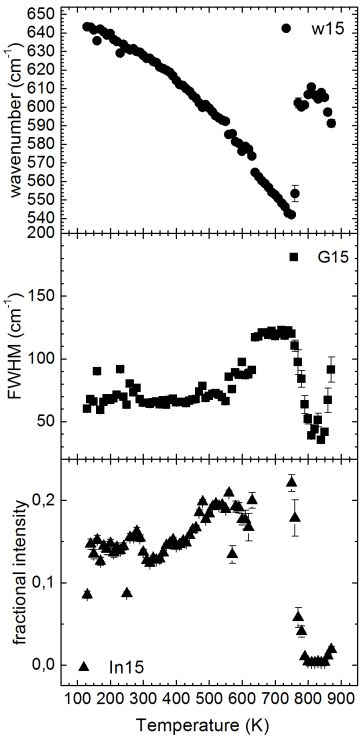

PT-P15

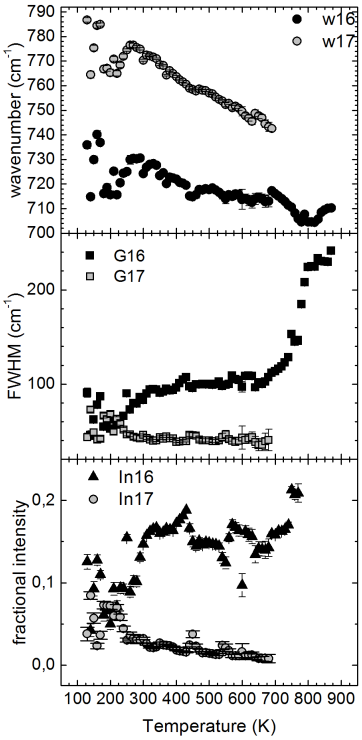

PT-P16-P17

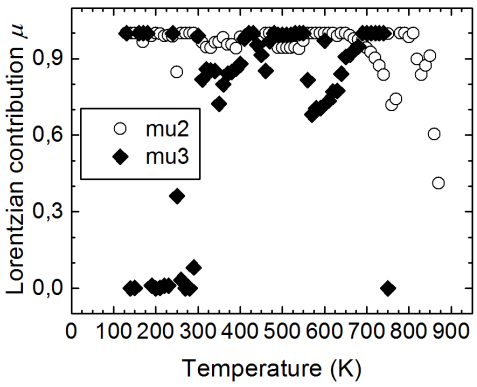

PT-P2-P3 Lorentzian contribution

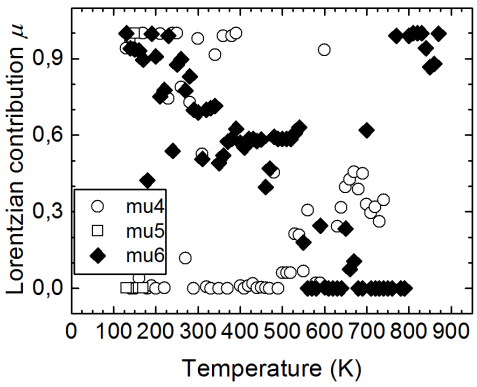

PT-P4-P5-P6 Lorentzian contribution

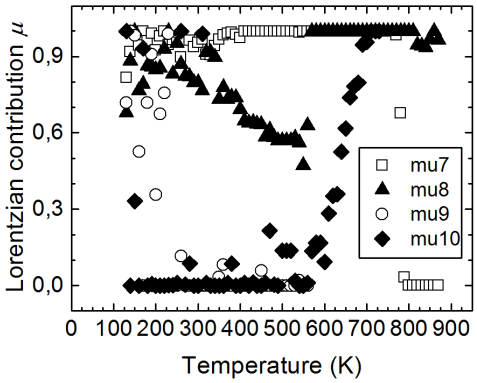

PT-P7-P8-P9-P10 Lorentzian contribution

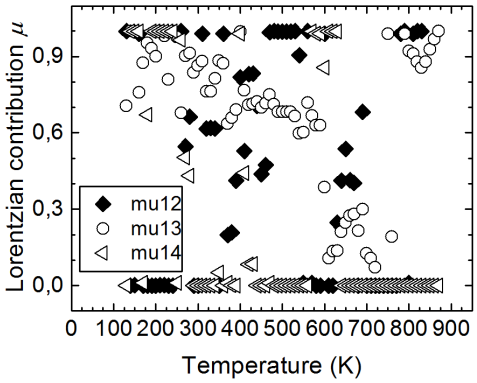

PT-P12-P13-P14 Lorentzian contribution

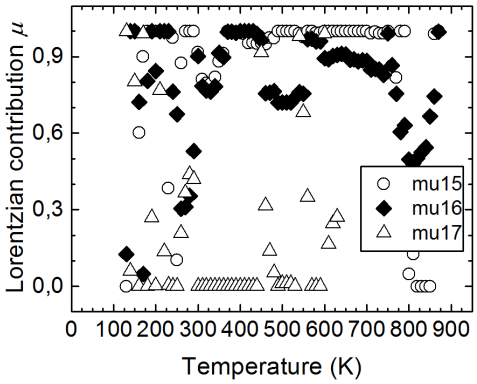

PT-P15-P16-P17 Lorentzian contribution

Versicherung an Eides statt

Hiermit versichere ich an Eides statt, dass ich die vorliegende Arbeit im Studiengang Geowissenschaften B.Sc. selbstständig verfasst und keine anderen als die angegebenen Hilfsmittel - insbesondere keine im Quellenverzeichnis nicht benannten Internet-Quellen - benutzt habe. Alle Stellen, die wörtlich oder sinngemäß aus Veröffentlichungen entnommen wurden, sind als solche kenntlich gemacht. Ich versichere weiterhin, dass ich die Arbeit vorher nicht in einem anderen Prüfungsverfahren eingereicht habe und die eingereichte schriftliche Fassung der auf dem elektronischen Speichermedium entspricht.

Hamburg, _____